Nuclear Organization in Cutaneous Anaplastic Large Cell Lymphomas

By

Ata Baslik

A Thesis submitted to the Faculty of Graduate Studies of

The University of Manitoba

in partial fulfilment of the requirements of the degree of

MASTER OF SCIENCE

Department of Physiology and Pathophysiology

University of Manitoba

Winnipeg

Abstract

Genomes of eukaryotic cells are organized in 3D non-random multiscale structures that have significant effects on function of their genome, of the cell and collectively with other cells, function of the entire organism. Through deregulation of genome maintenance pathways, diseased cells become susceptible to accumulate mutations and can remodel the structure of their genome over time to ultimately gain phenotypes that advance their pathology. A state of high mutation rate is a hallmark of cancer called genomic instability. As an early disease feature that drives cancer evolution, genomic instability has been investigated in multiple settings. A driver of genomic instability is dysfunctional telomeres. These are repetitive DNA 'TTAGGG' sequences that protect chromosomal ends of healthy cells. Dysfunctional telomeres can fuse with other telomeres, in cancer, this causes events that results in broken and then rearranged chromosomes when cells attempt to divide with fused chromosomes. Telomere function requires interactions with multiple nuclear proteins that help maintain its structure and position; one such protein is lamin A/C. This protein plays key roles in genome organization and is part of a 3D protein structure called the nuclear lamina that envelopes the nucleus. Studies have identified remodelling of 3D telomere profiles and lamin A/C dysregulation in various cancers and they are found to be associated with lymphoid malignancies including Hodgkin's Lymphoma, multiple myeloma, chronic lymphoid leukemia, and myelodysplastic syndromes. A disease where we so far lack understanding of genome remodelling and genome instability to the same extent as in the ones cited above is cutaneous anaplastic large cell lymphoma (C-ALCL), a lymphoid malignancy with relatively good prognosis. My project aimed to investigate changing 3D telomere profiles and lamin A/C expression in C-ALCL as it progressed through a malignant transformation. Results here show a heterogenous multifaceted telomere remodelling and lamin A/C deregulation associated with disease progression. Conclusions of this study offer an understanding of genomic alterations that drive transformation of a disease such as C-ALCL and serve as a building block to future studies that will help us understand what makes C-ALCL more treatable compared to other lymphoid malignancies.

Table of contents

List of Tables

List of Figures

Introduction

A brief history of the non-random organization of nucleus

In the later 1870s, Oscar Hertwig had demonstrated, through studies of sea urchin eggs, that, after fertilization, one male and one female pronucleus would become visible and then merge into a single nucleus (Hertwig, 1876; Hertwig, 1877; Hertwig,1878). This was later built on by Édouard van Beneden, who introduced the horse roundworm as a biological model in 1883 (van Beneden, 1883). This species possessed one (*A.m. univalens*) or two (*A.m. bivalens*) pairs of large chromosomes, which could be counted easily, allowing van Beneden to convincingly demonstrate that the number and size of chromosomes contributed by male and female pronuclei were equal in this fusion. This evidence led Oscar Hertwig and August Weismann, the latter who was also developing his chromosome theory of heredity, as well as some of their contemporaries, to conclude that the nucleus contained hereditary material. Their view was not to find general acceptance for decades to come. An immediate problem was the question of how, hereditary material, locked away with chromosomes in the nucleus, could dictate the functions of a cell.

In 1885, Carl Rabl published his work with mitotic cells from *Salamandra maculata* wherein he discussed an observation: chromosomal middles and ends showed similar polarization at the beginning and end of mitosis in these cells (Rabl,1885). He then hypothesized that chromosome structure could be maintained to an extent during interphase. Then in 1887, Theodor Boveri made an interesting observation while again working with the horse roundworm: Chromosomes appeared large in germ lines, but in somatic lines chromosome edges would remain visibly attached to nuclear membrane while their middles would dissolve. The extent to which chromosomes would disintegrate in the interphase cell nucleus or maintain a rigid structure became a controversy in this period (for a review of scientific paradigms in this period: Cremer & Cremer, 2006). Oscar Hertwig, for example, supported a view that, during the formation of the diploid cell nucleus, all material from male and female pronucleus would completely mix (Hertwig and Hertwig, 1887).

In 1909, Theodor Boveri coined the term *chromosome territory* to describe a hypothesis whereby chromosomes could transform into a “sponge of chromatin bundles” at the beginning of

interphase but, instead of mixing together, they would maintain that nuclear position (their *territory*) until they aggregated into their mitotic chromosome form once again for cell division (Boveri, 1909). This hypothesis also necessitated an interchromatin space (the name "interchromatin space" was first used 60 years later (Monneron & Bernhard, 1969) so the chromosomes would not get entangled. For Boveri, this mechanism was necessary for successful cell division. This was the first hypothesis that described a cellular nuclear architecture with functional purpose.

Boveri used fixed 2 and 4 cell horse roundworm embryos to test his hypothesis. Comparing chromosomes at the end of 1st mitosis (before they dissolved) and at prophase at the beginning of 2nd mitosis (just when they appear again) demonstrated quite similar positions and orientations (Boveri, 1909). Boveri was able to generate conclusive evidence towards his chromosome individuality and heredity theories (Boveri, 1909) but, at the time, tools necessary to tag individual interphase chromosome positions were not available. This led to a disregard of chromosome territories from 1950s to 1980s, until the necessary modern techniques were developed and used to validate his concept, which is largely accepted today.

As the 20th century progressed, newly developed techniques of molecular biology were applied to extensively study the cell nucleus. However, investigation of DNA sequences and transcription factors was far more prioritized compared to structural investigation of protein complexes and DNA at nucleosome levels, while investigations of high order chromatin architecture and chromatin positioning were near nonexistent (Cremer *et al.*, 2014). Until the early 1980s, most nuclear biologists were still content with a view of chromatin particles randomly mixed as spaghetti during interphase.

The non-random nature of chromatin organization at multiple scales during interphase has been gradually accepted in the last 30-40 years. With this understanding new fields of studies have come: 3D and later 4D nucleome research (https://commonfund.nih.gov/4Dnucleome), as well as a complete appreciation for links of nuclear structure and function, starting from single molecules up to the chromosome territories (for review, Cremer *et al.*, 2015).

Architectural features of the genome

Chromatin structures

Eukaryotic genomes are organized through some ubiquitous architectural features of increasing complexity: at the smallest level right after the DNA helix is the chromatin fiber. 146 base pairs (bp) of DNA are wrapped around an octamer complex of core histone proteins: the nucleosome. Nucleosomes then can dynamically coil and straighten back to varying degrees to form chromatin fibers which have diameters ranging between 5-24 nanometers (nm) throughout the nucleus (for review see Maeshima *et al.,* 2019). The degree of compaction is adjusted depending on access to DNA required by regulatory proteins. The chromatin fiber can also form loops, an architectural feature formed with kilobase pairs to megabase pairs of fiber, which can bring sequentially distant regulatory elements such as enhancers or silencers to stable 3D proximity with genes and promoters where they can work together (for reviews, Vermunt *et al.,* 2018; Dekker & Misteli, 2015). Chromatin looping was initially identified by development of chromatin capture techniques and was later confirmed by other methods.

Chromatin capture techniques have been frequently used for studies of genomic architectural features so it is worthwhile to briefly introduce the principle of these methods here: During chromatin looping, a chromatin fiber directly touches another chromatin fiber and they can be chemically crosslinked at that point with an agent such as formaldehyde. Chromatin is then digested with a restriction enzyme. Cross linked segments can be then ligated and quantified with various methods. The sequence of these segments will reveal genome wide interactions (Dekker *et al.,* 2002, for review Dekker & Misteli, 2015).

Chromatin domains are more complex architectural features relative to chromatin loops (for review, Misteli 2020). They are often several hundred kilobases in size (Fudenberg *et al.,* 2016). Although extensively studied using chromatin capture techniques, these structures were first observed with Fluorescence *in situ* hybridization (FISH) experiments (Shopland *et al.,* 2006). Chromatin domains eventually came to be referred as topologically associated domains (TADs) because of their preference to interact with each other. The formation of TADs is a directed and ATP-dependant process which starts with a chromatin loop-extrusion (Fudenberg *et al.,* 2016). After extrusion, the loop then forms many internal folds and smaller loops via self organization which give a 3D shape to the TAD. The functional significance of TADs is still to

be determined; however, they could be working, at least to an extent, as coregulatory units by restricting a selection of genes, transcription factors and enhancers to a 3D space where they can work together (Beagrie *et al.*, 2017). Currently, they are primarily considered to work as an assisting structural base to other gene regulating chromatin-chromatin or protein-chromatin interactions (Misteli, 2020).

FISH methods can visualize multiple TADs attaching to form even more complex 3D structures (Wang *et al.*, 2017). These multiple megabases spanning units are called chromatin compartments. It is also possible to observe chromatin compartments by quantifying interactions between TADs with chromatin capture techniques (Fraser *et al.*, 2015). The largest units of genome organization are chromosome territories, which are made up of the entire DNA of a single chromosome and contain multiple chromatin compartments that are interacting.

During interphase, the DNA from a chromosome will occupy a restricted space of the nucleus called a chromosome territory (for review, Cremer & Cremer, 2010). Although chromosome territories were proposed in the 1880s as discussed above, in the early 1980s, modern studies were beginning to re-establish this hypothesis. Using laser irradiation, small sections of interphase nuclei were exposed to DNA damage and then chased with tagged nucleic acids. When the tagged nucleic acids were then visualized in mitosis spreads, recent DNA repair was observed and found to be restricted to a single chromosome or a few chromosomes (Zorn *et al.*, 1979). If chromosomes completely dissolved and mixed during interphase, the expectation would have been small DNA repair tags along many different chromosomes. Still, the consensus shift towards accepting these macro nuclear architectures can be traced to later 1980s, some 100 years after they were first proposed by Carl Rabl, due to the development of "chromosome painting" which finally allowed for direct visualization of chromosome territories in interphase nuclei using libraries of FISH probes (Lichter *et al.*, 1988).

Preceding our understanding of large structural chromatin units, the most clear observation suggesting a non-random nature of nuclear organization was the spatial separation of transcriptionally active euchromatin from condensed inactive heterochromatin (Fawcett 1966, Ferreira *et al.*, 1997). This separation is also evident when genome wide interactions of active and inactive loci are quantified with chromatin capture, which results in mapping the 2 corresponding spatially segregated interaction groups called A and B compartments (Lieberman-

Aiden *et al.,* 2009; for review Rowley & Corces, 2018). Another cytological observation was that heterochromatin would be generally located at the nuclear periphery while euchromatin would be positioned at the nuclear interior (Fawcett 1966). This led to propositions of a correlation between transcriptional silencing and positioning at the nuclear periphery (Sadoni *et al.,* 1999).

Nuclear envelope

At the nuclear periphery, the nuclear envelope acts as an immobile and constraining structure in genome organization compared to the dynamic and locally diffusing chromatin. The interior of the nuclear membrane is lined with the nuclear lamina; a meshwork structure where the principal components are the A and B-type lamin proteins, which are intermediate filaments, and lamin-associated proteins (for review Shevelyov & Ulianov, 2019).

Chromatin capture techniques have demonstrated that in various organisms' genomes, including the human genome, there are specific chromosomal regions that attach to the nuclear lamina. These regions, named lamina-associated domains (LADs), are indeed gene poor and the relatively few genes they contain are weakly expressed or silent genes. This is consistent with the observation of regular peripheral positioning of heterochromatin (Fawcett, 1966). Multiple studies have identified proteins that are chromatin interacting and/or part of the nuclear envelope. Some of these proteins are demonstrated to be playing a role in this heterochromatin tethering (Shevelyov & Ulianov, 2019). Researchers most commonly investigate this function by depleting one or multiple target proteins and then following up with FISH to see if LADs, at least to some extent, get detached from the nuclear envelope. The chromatin attaching role of these proteins is usually specific to organisms, cell types and the developmental stage of the cell. Lamins for example can be necessary for tethering: knockout of *Lmna* gene, which codes for lamin A/C proteins, causes a shift of heterochromatin to nuclear interior and euchromatin to periphery in post mitotic mouse cells that also lack the protein Lamin-B-Receptor (LBR) (Solovei *et al.,* 2013). In mouse embryonic stem cells (mESCs), however, loss of all lamin proteins only leads to detachment of some LADs and no heterochromatin-euchromatin inversion occurs, indicating existence of other interactions that maintain the chromatin positions of most LADs (Zheng *et al.,* 2018).

Artificially tethering gene loci to the nuclear periphery leads to their inactivation or if they were already silent, to their resistance to later activation (Kumaran & Spector, 2008; Finlan *et al.,* 2008; Reddy *et al.,* 2008; Wang *et al.,* 2018). Therefore, genes can be repressed by mechanisms independent of the nuclear lamina and be positioned towards the nuclear lamina because of their repression, but they can also be repressed by the nuclear lamina because of their contact with it. However, a dedicated localization machinery which repositions to-be-silenced genes to the nuclear lamina has not been identified (Misteli 2020). Currently, silenced genes are believed to position to the periphery because of their functional status, where the nuclear lamina exerts a further robustness to the repression (Shevelyov & Ulianov, 2019).

3D positioning of chromatin according to its functional status is also evident at the most complex level. Chromosome territories show a similar non-random pattern to genes but with their own set of rules and exceptions. In human lymphocytes, it was shown that gene density correlates with radial position of chromosomes: for example, gene dense human chromosome 19 is located to the nuclear interior, while gene poor human chromosome 18 prefers a peripheral position despite the chromosomes having a similar size (Boyle *et al.,* 2001; Cremer and Cremer, 2001a). This arrangement is conserved during evolution (Tanabe *et al.,* 2002). This is again consistent with observations that heterochromatin is localized to the periphery and euchromatin is localized to the interior (Fawcett 1966). For human fibroblasts, unlike the lymphocytes, chromosome size is also a factor of chromosome position where smaller chromosomes are positioned more to the nuclear interior (Bolzer *et al.,* 2005).

Nuclear organization of telomeres

Telomeres are the protective repetitive terminal sequences of chromosomes and responsible for chromosomal integrity; they are also both organizers of genome as well as dependant on nuclear organization for their own functions (for review Burla *et al.,* 2016). Mammalian telomeres contain arrays of $(TTAGGG)_n$ repeats and end with a single 3’ G-rich overhang. Healthy telomeres form their own unique 3D architectural motifs; the ending 3’ single strand overhang bends into what is called a t-loop and invades the preceding telomeric double strand. Telomeric double strand folds open to allow the overhang single strand to invade and hybridize with one of its halves, the other non hybridized telomeric strand, now loose, forms

what is called a displacement loop (D-loop) (Griffith *et al.,* 1999). Telomeres can have non-random 3D nuclear positions; in many organisms a typical organization, called a 'bouquet', is observed during the first meiotic prophase of development, during which chromosome ends are attached to the periphery (Scherthan *et al.,* 2000). In somatic interphase cells, telomeres are not localized to a specific location (Crabbe *et al.,* 2012), but multiple direct and indirect interactions have been identified between telomeric DNA, telomere associated proteins and proteins associated with nuclear lamina/envelope (for review Burla *et al.,* 2016). A-type lamins are important partners that play key roles in the maintenance of telomere length, internal structure, nuclear positioning and thereby telomere function. Quantifying telomere motion reveals they display a slow anomalous diffusion in mammalian interphase cells; however, upon depletion of lamin A, their motion transforms to fast and normal diffusion (Bronshtein *et al.,* 2015). Loss of lamin A directly results in telomere shortening (Gonzalez-Suarez *et al.,* 2009) as well as an inability to process dysfunctional telomeres with the nonhomologous end joining (NHEJ) DNA repair pathway (Gonzalez-Suarez, Redwood, Perkins, *et al.,* 2009). 3D Telomere positions are dependant on cellular shape as well as cell cycle dependant, as telomeres can be observed to form a disc when chromosomes are aligning in G2 phase before M phase (Chuang et al. 2004, Vermolen, 2005). It is therefore possible to determine the cell cycle phase based on a quantification of 3D telomere position.

Measuring genome organization

It is possible to quantitatively measure aspects of 2D, 3D and even 4D genome organization through various techniques that can be separated into imaging and chromatin conformation capture (3C) based methods, although recently boundary pushing techniques are being developed that do not fit in either category (for review Kempfer & Pombo, 2019).

Chromatin capture

Conformation capture techniques, specifically the more recent Hi-C, are powerful in their capacity to simultaneously detect all genome-wide chromatin-chromatin contacts and generate a nuclear structure map with enormous data. These methods also have important limitations due to their proximity ligation-based approach that has difficulty capturing long-range interactions and interactions between more than 2 loci. Random and intermolecular ligations (between non-crosslinked DNA fragments) are major sources of noise in these methods (Kong & Zhang, 2019). The interactions should be therefore validated by an independent method such as FISH (Simonis *et al.,* 2007). Chromosome territories and their shapes can still be inferred by chromatin capture, appearing as high frequency of contacts within a chromosome, while intrachromosomal contacts allow for an understanding of chromosomal 3D positioning relative to each other (Spilianakis *et al.,* 2005; Nagano *et al.,* 2017). The sizes of smaller sized chromatin architecture such as TADs match very well with the resolution of 3C based approaches allowing for their collective detection, even sub-TAD loop structures within can be identified (Rao *et al.,* 2015). Single cell methods have also been developed (Nagano *et al.,* 2015; Kempfer & Pombo, 2019).

Microscopy

Microscopy, on the other hand, has the capacity to detect a great range of interactions between proteins, DNA and RNA but is so far limited to being able to observe targets determined by researchers before the experiment (Kempfer & Pombo, 2019). Microscopy can also provide loci locations relative to nuclear bodies and periphery. DNA-FISH specifically has been used extensively in the field of 3D genomics due to its capacity to show 3D locations of genes and chromosomes (Speicher *et al.,* 1996). This advantage has been built upon by modern techniques such as sequential FISH (seqFISh) approaches that create barcodes for loci through repeated rounds of hybridization (Lubeck *et al.,* 2014; Shah *et al.,* 2016; Takei *et al.,* 2017). Recently, FISH has been used to detect thousands of individual loci in single cells, which were then integrated by computation to generate 3D spatial maps of every chromosome territory and thousands of alleles, combined with a view of how their DNA sequence takes 3D shape (Takei *et al.,* 2021). This information has also been further integrated with sequential immunofluorescence to see how proteins such as chromatin markers and nuclear substructures position alongside DNA and RNA (Takei *et al.,* 2021). Microscopy offers the advantage of detection of long-range

interactions between loci that are beyond the range of chemical ligation and, more recently, the capacity to study the nuclear organization of live cells (Ma *et al.,* 2016).

Measures of genome organization

Some aspects of nuclear organization include the non-random 3D locations of specific genes and chromosomes, telomeres, heterochromatin, euchromatin and nuclear bodies which can all be measured relative to the nuclear center/periphery and/or each other, using variations of the methods mentioned above. 3D location is not the only measurable aspect of nuclear organization, some studies for instance have quantified genome wide chromatin compaction (Young *et al.,* 1986; Righolt *et al.,* 2014; Boettiger *et al.,* 2016) or chromosome orientation (Schmälter *et al.,* 2014; Schmälter et al. 2015). To study alterations, these measurements of nuclear organization can then be compared between disease states and healthy cells, different developmental stages of a cell, between cell types or cells of same type from different organisms (Krijger and de Laat 2016, Spielmann *et al.,* 2018, Dekker *et al.,* 2017).

Genomic Instability and Cancer

Healthy cells invest significant resources to the maintenance of their genome, this results in species-defining stable features such as what is known as karyotype: Healthy somatic cells in an individual multicellular organism contain a constant number of chromosomes (or multiples of a constant number). Any deviation from this expected count, as well as partial gains or losses, is termed as aneuploidy. The rate of mutations is also kept under strict control unless functionally necessary. In humans for example, chances of acquiring a mutation that would alter a protein coding region of genome is less than one per generation (Keightley, 2012).

It was noted more than a century ago that cancer cells would tend to not adhere to the chromosomal homogeneity of their organism (Von Hansemann, 1908). Boveri was the first to hypothesize that abnormal growth of cancer cells could be due to this aneuploidy (Boveri, 1914). This feature of continuously developing aneuploidy as well as chromosomal rearrangements like translocations and inversions, later called chromosomal instability (CIN), have been observed

very commonly in cancers. CIN can be categorized between structural CIN (sCIN) and numerical CIN (nCIN). Structural CIN can occur, for example, due to high rate of balanced translocations between chromosomes which do not change copy numbers but cause a karyotype alteration. Numerical CIN can be due to, for example, a high rate of segregation mistakes during anaphase that causes changes to chromosome counts but no rearrangements between them (Bayani *et al.,* 2007). Some genomic events, such as unbalanced translocations, can lead to both at the same time. sCIN and nCIN are therefore commonly observed together (Bayani *et al.,* 2007). Both sCIN and nCIN are in fact specific forms of genomic instability, which is a hallmark of cancer that, although known previously, emerged to greater importance in the 2000s (for reviews of genomic instability Negrini *et al.,* 2010, hallmarks of cancer; Hanahan & Weinberg, 2011).

Genomic instability refers to the rate of mutations accumulating in a cellular lineage. This can be in the form of chromosomal abnormalities. Genomic instability can also be in form of increased frequency of base pair mutations, called Nucleotide Instability (NIN), or changes in number of noncoding microsatellite sequence repeats, defined as Microsatellite Instability (MIN) (for MIN review, Li *et al.,* 2020).

Genomic instability has been described as an enabling hallmark of cancer in that it generally precedes and is crucial to the acquisition of other hallmarks (Hanahan & Weinberg, 2011). Eventually, some mutation accumulating cells will acquire phenotypic alterations that benefit their selective potential in a specific tissue microenvironment. This leads to the new subclone(s) expanding and eventually dominating its sister cells. Successor clonal expansions will continue with new mutations, if they add a trait that infers a selective advantage, which contributes to the oncogenic potential of the cell population in a multistep tumor evolution. A most common example that occurs in almost every type of cancer is inactivating mutations of *TP53* which codes for p53, a critical tumor suppressor (Olivier *et al.,* 2009). The prevalence of these mutations varies greatly from 5% for cervical cancer cases to 50% of ovary cancers and is more common in late-stage disease (Olivier *et al.,* 2009).

Genomic instability itself is usually a cause of mutations that lead to dysfunctions in genome maintenance and/or increase sensitivity to mutagenic stress. The most striking examples of this phenomenon are hereditary cancer risk factors: Werner syndrome helicase (WRN), breast

cancer type 1 susceptibility protein (BRCA1), breast cancer type 2 susceptibility protein (BRCA2) and its partner PALB2, RecQ protein-like 4 (RECQL4), Nijmegen breakage syndrome protein 1 (NBS1) are all known to have DNA repair functions and inherited mutations of these proteins makes individuals predisposed to development of various cancers, attributable to resulting genomic instability (Ripperger *et al.,* 2008; Bachrati and Hickson, 2003; Kennedy and D'Andrea, 2006).

Due to telomere shortening during DNA replication, the proliferative potential of cells is limited by their telomere lengths (Shay & Wright, 2000). Another hallmark of cancer is achieving what is known as replicative immortality, typically by expressing telomerase and/or, less commonly, alternative mechanisms of telomere elongation (Hanahan & Weinberg, 2011). Aside from limiting proliferation, critically short telomeres also lack sufficient shielding from their partner proteins that prevent them from being recognized as double strand breaks (DSB) by DNA repair mechanisms (van Steensel *et al.,* 1998, Liddiard *et al.,* 2016, Rai *et al.,* 2010). Telomeres processed with NHEJ can make fusions either head-to-head with other telomeres of other chromosomes (or telomeres from sister chromatids) or previously broken non-telomeric genome loci. This creates dicentric or Robertsonian chromosomes as well as unbalanced translocation chromosomes. Dicentric chromosomes can break during cell division and cause further fusions in a process called breakage-fusion-bridge (BFB) cycle. This process fosters chromosomal translocations and partial amplifications by DNA repair pathways, which can dramatically reorganize the genome architecture in a single event. It also initiates an ongoing genomic instability that can last many cell cycles until chromosomes stabilise. Early in cancer progression, mostly prior to activating telomere maintenance pathways, pre-malignant proliferating cells commonly experience BFB cycles (Kolquist *et al.,* 1998; for review Mai, 2010). Although BFB cycles might appear to be a problem for the cell, for cancer cells it appears this telomere-driven genomic instability can greatly contribute to acquiring oncogenic traits early on in the disease by creating copy gains and losses (Cleal *et al.,* 2018).

Genomic instability can greatly reorganize the 3D nucleus at multiple levels (for review; Krijger and de Laat, 2016). Large chromosomal rearrangements not only alter chromosome territories but can also delete, rearrange the borders of, and create *de novo* TADs (examples include Sathitruangsak *et al.,* 2016; Marella *et al.,* 2009; Sanborn *et al.,* 2016; Guo *et al.,* 2015).

Point mutations can deactivate enhancers or create new transcription factor binding sites on enhancers, which disrupt or generate new loop formations with genes, respectively (Lettice, 2003; Fukami *et al.,* 2012). Furthermore, reorganization of the 3D nucleus by genomic instability can have contributions to the cancerous potential of cells: in Burkitt's lymphoma, due to a t(8;14) translocation, MYC oncogene is placed under the control of immunoglobulin heavy chain enhancer (Taub *et al.,* 1982); in medulloblastoma, rearrangements create new interactions with super-enhancers for the GFI1 gene family (Northcott *et al.,* 2014).

Measures of genomic instability

The existence of genomic alterations alone does not mean a cell has genomic instability (Lengauer *et al.,* 1998). Individuals with Down Syndrome, for example, have all their cells contain a chromosomal abnormality, trisomy 21, but their cells normally do not have genomic instability (Antonarakis *et al.,* 2004). Genomic instability refers to a rate and not a state; it means genomic alterations must be occurring at a pace greater than normal. Ideally therefore, studies that measure true genomic instability will attempt to measure a ground state and then do time-based measurements to quantify a rate of mutations occurring in deviation from that ground state. For example, in 2002, Bunz *et al*. investigated whether p53 loss leads to CIN by culturing wild type and p53 knockout cell lines, which initially had the same karyotype, in parallel (Bunz *et al.,* 2002). They observed karyotype using multiplex FISH after 25 generations, then compared it to the initial karyotype to determine a rate of chromosome losses, gains, and rearrangements. They detected no significant rate difference, reaching the conclusion that p53 loss alone does not lead to CIN *in vitro*.

However, both for research and for clinical purposes, especially when repeated biopsies are unavailable and/or cell culture is not an option, directly characterizing actual rate of alterations in disease may not be possible (Geigl *et al.,* 2008). Therefore, researchers and clinicians use a set of surrogate measures that indicate genomic instability or correlate with it. Measurements of cell-to-cell variability in genome organization from a static single sample snapshot is a reliable indicator of ongoing genomic instability (Geigl *et al.,* 2008). Researchers may focus on CIN, nucleotide instability (NIN) or microsatellite instability (MIN); since they are all types of genomic instability (that are often in interplay), measure of one sufficiently

identifies at least the existence of genomic instability (Pikor *et al.*, 2013).

While it is not a commonly used technique to assess genomic instability, single-cell whole-genome sequencing would, in theory, generate the most comprehensive insights for this purpose, being able to detect chromosomal copy number changes, inversions, and translocations; as well as nucleotide substitutions, insertions or deletions and microsatellite expansion or contraction. Historically a much more commonly used technique is Trypsin-Giemsa staining of metaphase chromosomes, which creates chromosome specific patterns that can be used to identify CIN but not NIN or MIN. More recently, spectral karyotyping (SKY) metaphase cells, which is a technique that uniquely paints each chromosome, has been an excellent choice for detecting CIN (Bayani & Squire, 2001). Metaphase cells are greatly outnumbered by interphase cells even in most proliferating tumors and culturing samples even short-term could add new genome alterations, both of which pose a limitation. These could be overcome by using telomere FISH, where the count of telomeres can be used as an indicator of aneuploidy during interphase (Louis *et al.*, 2005, Vermolen *et al.*, 2005). Different techniques, such as Flow cytometry, PCR, array Comparative Genomic Hybridization (aCGH) and others, offer their own strengths and limitations in studying genomic instability (for review, Pikor *et al.*, 2013).

Lymphoid and other hematological malignancies

Hematological malignancies are groups of tumors of blood forming immune cells, sometimes also referred to as liquid tumors because they can be easily observed in circulation. The included classifications are lymphomas (cancers of lymphocytes, mainly located in lymph nodes), leukemias (mainly located to blood and bone marrow) and myelomas (which are cancers of plasma cells that produce abnormal antibodies). In this subsection, I detail their pathophysiology specifically in the context of nuclear organization and genomic instability.

Solid tumors sometimes have chromosomal abnormalities that can contribute significantly to their pathogenesis (Mitelman *et al.*, 2007). For hematological malignancies, chromosomal abnormalities are even more common (Küppers, 2005). For lymphoid malignancies specifically, chromosomal abnormalities are the most frequent form of mutation (Küppers, 2005). This is attributable to the predisposition of T and B cells to having chromosomal abnormalities, as these cells make programmed short-term use of genomic

instability to create the necessary variation in their immune repertoire. Immunoglobulin chains and T Cell Receptor (TCR) genes are constructed through a selection of Variable, Diversity, and Joining [V(D)J] regions by recombination. B cells go on to make use of somatic hypermutation and class-switch recombination to adjust their antibody production to the specific needs of the current immune defense (Küppers, 2005; Nussenzweig & Nussenzweig, 2010). This reliance on genomic instability is considered to account for the fact that 95% of lymphomas are of B cell origin (Küppers, 2005), because, self-inflicted DNA breaks and editing are error-prone tools for creating protein variations. In B cell malignancies, immunoglobulin heavy chain (*IgH*) loci on chromosome 14 appears to be a very common site for chromosomal translocations which are considered to be [V(D)J] recombination mistakes made early in cell development (Bouamar *et al.,* 2013). Aberrant somatic hypermutation can cause translocations that affect proto-oncogenes responsible for causing diffuse large B cell lymphoma (Pasqualucci *et al.,* 2001).

Telomere dysfunction driven BFB cycles due to extremely short telomeres is implicated in a source of CIN in lymphoid malignancies (Krem *et al.,* 2015). In Hodgkin's lymphoma (HL), an ongoing erosion and spatial disturbance of telomeres is evident in Hodgkin cells (H cells) which transition to end stage Reed– Sternberg cells (RS cells) (Knecht *et al.,* 2009). This telomeric shift is also accompanied by increasing BFB cycles and increasing complexity of chromosomal abnormalities during the H to RS cell evolution (Guffei *et al.,* 2010).

Significance of altered genome organization in a clinical scenario

Commonly observed altered nuclear organization in cancers has had a clinically significant impact on diagnosis, prognosis, and treatment choices especially with liquid tumors which can be easily collected. In general, CIN is correlated with negative outcomes for both B- and T-cell malignancies (Krijger and de Laat 2016) but, based on disease, more complex trends can be observed, such as in Acute Lymphoblastic Leukemia/Lymphoma (ALL). In ALL, whole chromosome losses correlate to a poor prognosis of 40% or less 5-year survival rate, this prognosis gets worse the fewer chromosomes there are (Harrison et al, 2004). Chromosome gains on the other hand confer to an up to 90% 5-year survival rate in ALL (Harrison et al, 2004).

Telomere length can be correlative with prognosis as well. Shorter telomeres in HL are

associated with resistance to chemotherapy and the probability of secondary cancer (Knecht *et al.,* 2012; M'kacher *et al.,* 2007). In Chronic lymphocytic leukaemia/small lymphocytic lymphoma (CLL), telomeres shorter than 5 kB correlate with reduced overall survival rate for the patient (Lobetti-Bodoni *et al.,* 2010).

Lamin A/C plays a role in supporting telomere function and acts as a nuclear organizer. Lamin A/C has been implicated in lymphoid malignancies as well as in other cancers (for review; Dubik & Mai, 2020). Immunostaining studies have not found lamin A/C expression at observable levels for resting B cells (Contu *et al.,* 2018) and have found a minimal amount only in a small subset of resting T cells (González-Granado *et al.,* 2014). Upon activation, both T and B lymphocytes upregulate lamin A/C (Contu *et al.,* 2018; González-Granado *et al.,* 2014). Cancer cells frequently under- or over-express lamin A/C, sometimes with expression heterogeneity between tumor samples of a disease type (Dubik & Mai, 2020). The expression patterns can be clinically significant, such as in diffuse large B-cell lymphomas where the lamin A/C promoter was found to be epigenetically inactivated in 34% (14/41) of cases and this silencing also correlated with poor outcome (Agrelo *et al.,* 2005). The large variation of lamin A/C expression patterns in cancers combined with various known functions of lamin A/C in different tissues can make establishing a link between cancer phenotype and lamin A/C associated genome remodelling difficult. Looking beyond expression can strengthen our understanding as lamin A/C is also often found to have abnormal nuclear localization and structures in cancer (Moss *et al.,* 1999; Foster *et al.,* 2011). Once again in HL, both H cells and RS cells strongly express lamin A/C, as observed in both culture of HL cell lines and in tissue samples (Contu *et al.,* 2018). Lamin A/C also forms structures inside the nucleus that divide the nucleus into compartments in HL. Disrupting lamin A/C expression by RNA interference leads to a failure of H cells to transition into multinuclear RS cells, accompanied by a spatial reorganization of H cells' telomere positions and shortening of their telomeres (Contu *et al.,* 2018). The evidence shows nuclear remodeling linked to lamin A/C dysregulation can be a factor in cancer progression. Possibly H cells need lamin A/C to keep telomere driven BFB cycles at a sustainable level or else genomic instability becomes too much for them to progress to RS cells. It is also possible that the multi-nucleation process is impossible without lamin A/C.

With regard to guiding therapeutic choices, a viable strategy for targeting cancers with a

high genomic instability phenotype is to increase additional genomic instability to a level unsustainable for cancer cells. Several classic cancer therapies rely at least partially on this strategy. DNA damaging compounds, like cisplatin, have more cytotoxic potential if the DNA repair pathways of target cells are less functional (Dasari & Bernard Tchounwou, 2014). Microtubule targeting taxanes, like paclitaxel, lead to failure of chromosomal segregation during cell division and aim to increase existing chromosomal abnormalities to lethal levels (Wordeman & Vicente, 2021). In lymphoid malignancies as well as in all other diseases, the efficacy of these therapies depends on how well they target the specific mutations and specific weaknesses in genome maintenance of the underlying disease. Poly(ADP-ribose) polymerase (PARP) plays a role in recruiting DNA repair machinery and its inhibition induces DSBs that selectively kill cells with other already faulty components of DNA repair pathways (Dziadkowiec *et al.,* 2016). PARP inhibitors, like Olaparib, are approved for treating particularly BRCA (Homologous DNA repair) mutated patients, with ovarian and breast cancer. Olaparib is currently in a precision medicine phase 2 trial against non-Hodgkin's lymphomas that are screened for ATM, BRCA1, BRCA2, RAD51C, RAD51D mutations, which are factors contributing to homologous DNA repair (Clinical trial NCT03233204). Attacking telomere driven genomic instability is another strategy. BIBR1532, a telomerase inhibitor, selectively kills leukemia cells independently of their telomere lengths. This lethality is believed to be driven by an exacerbation of telomere dissociation with telomere capping proteins (Damm, 2001 *et al.*; El-Daly *et al.,* 2005). BIBR1532 served as a proof of concept for the next generation telomerase inhibitors such as imetelstat, currently in phase 3 trials (NCT02598661, NCT04576156).

Cutaneous T cell lymphomas

Unlike most non-Hodgkin lymphomas (NHL), Cutaneous T Cell Lymphomas (CTCL) are a class of T cell origin cancers. They are named cutaneous because patients with these diseases present with skin rashes due to malignant T cells migrating to dermal tissue. Cutaneous T cell lymphomas are further divided into subclasses (Willemze, 2005). 30% of these are characterized by CD30 cell surface marker positivity. These include primary cutaneous anaplastic large cell lymphoma (C-ALCL) and lymphomatoid papulosis (LyP), which are parts of a single disease spectrum but named for different variations of clinical skin symptoms and

histological appearance (Willemze, 2005). Many cases are borderline between the two, based on histological appearance (Willemze, 2005). The prognosis is usually good for C-ALCL, with estimated 5-year survival exceeding 90%, which is much more favourable compared to other CTCLs (Bekkenk *et al.,* 2000). Some recurring chromosomal alterations have been characterized such as the gains on 6p, 7q, and 19, and losses on 6q, 9, 13 and 18 (Boni *et al.,* 2000; Mao *et al.,* 2003; van Kester *et al.,* 2010). Studies have reported these alterations to be fewer in comparison with other CTCL. Telomerase activity and generally long telomeres that are comparable to healthy cells are reported in C-ALCL (Chevret *et al.,* 2014). Genomic instability comparisons with other CTCL have not been undertaken as yet. Another group of CD30 positive CTCLs are mycosis fungoides (MF), which are diseases initially restricted to the skin that can later advance to Sezary Syndrome (SS), a leukemic form of CTCL (Willemze, 2005). Previous studies have found telomere loss and more short telomeres compared to control cells, a trend that was greater for advanced cases (Bienz *et al.,* 2021).

Mac cell lines

In my studies, I used three C-ALCL cell lines that originated from the same individual. They are Mac-1, Mac-2A and Mac-2B lines known to have a single clonal background but Mac-2A and Mac-2B are started at a later malignant disease stage (Davis *et al.,* 1992). Their case is detailed below. These lines present the opportunity to study a phenotype shift from indolent to aggressive cancer starting from a single clonal background. This opportunity has intrigued other research groups who identified various mutations attributed to this malignant cancer evolution (Knaus *et al.,* 1996; Levi *et al.,* 2000; Ehrentraut *et al.,* 2012; Ehrentraut *et al.,* 2016).

The case of Mac cell lines is summarised here: In 1971, a 31-year-old white male individual presented with skin rash (case report; Davis *et al.,* 1992). He was diagnosed by biopsy with mycosis fungoides, a form of CTCL, and given external radiation. In 1975, he developed abnormal sized lymph nodes and was diagnosed with HL. Radiotherapy resulted in a complete remission of HL, but skin lesions appeared and spontaneously disappeared for the next 8 years. In 1983, skin lesions were biopsied and diagnosed with lymphomatoid papulosis (LyP); the 1971 diagnosis was also then reinterpreted and changed to LyP. Lymph node biopsies showed a translocation, t(8;9)(p22;p24), in some 20% of the cells in metaphase. In 1985, circulating

abnormal cells (Sezary-like) were detectable and patient had an extended red skin rash (erythroderma). Skin biopsies revealed t(8;9)(p22;p24) containing CTCL cells. In 1987, ulcerating skin lesions developed that showed large cells. Patient passed away from complications in 1988 and lymph node analysis in autopsy identified C-ALCL. Analysis of chromosomal rearrangements later confirmed that some of the malignant cells observed through the whole 1971-1988 case were from a common T-cell clone (Davis *et al.,* 1992).

Three cell lines were initiated from this case: Cell line Mac-1 was started in 1985 from indolent cells in the peripheral blood, while cell lines Mac-2A and Mac-2B were started from separate aggressive skin-tumor nodules in 1987 taken on the same day.

Rationale, Hypothesis and Aims

Rationale

The 3D organization of the genome is found to be altered in lymphoid malignancies often in a clinically significant way, as explained above. C-ALCL is a disease where prognosis compares favourably to other CTCL and B cell lymphomas (Boni *et al.,* 2000; Mao *et al.,* 2003; van Kester *et al.,* 2010; Bekkenk *et al.,* 2000). C-ALCL has fewer chromosomal aberrations

compared to other CTCL and average telomere lengths that are comparable to healthy T cells (Chevret *et al.*, 2014). Together this could mean that compared to other lymphoid malignancies, telomere driven BFB cycles are not as prominent in C-ALCL and genomic instability is lower, a phenotype that is attributable to the good prognosis of this disease.

However, we still lack information on lengths of individual telomeres and cell-to-cell variability of telomere profiles in C-ALCL, as telomere FISH has not been applied to these questions. The 3D spatial positions of telomeres as well as existence of telomere aggregates have not been investigated in this disease so far. We also lack insight about how or if the telomere profile of C-ALCL changes when this disease does evolve to aggression.

Another component of nuclear organization that has not been investigated in C-ALCL is lamin A/C. Lamin A/C performs plays roles in heterochromatin function and gene localization by associating with LADs (Bronshtein *et al.*, 2015), as well as contributing to telomere function by interacting with telomere repeat-binding factor 2 (TRF2) and preventing associated BFB genomic instability (Kolquist *et al.*, 1998; Gonzalez-Suarez *et al.*, 2009; Wood et al., 2014; for BFB review Mai, 2010). In cancer, lamin A/C is often dysregulated. Furthermore, there is evidence that in HL, which is another lymphoid malignancy, lamin A/C can form abnormal internal structures and directly interfere with genome organization (Moss *et al.*, 1999; Foster *et al.*, 2011; Contu *et al.*, 2018). It is currently unknown if lamin A/C expression and structure is altered in C-ALCL. Any changes to expression and structural patterns lamin A/C might undergo through malignant cancer evolution have also not been investigated.

This study was designed to address these gaps in our current knowledge, detailed above. In summary, I, guided by my supervisor, considered that the telomere profiles and expression/structure of lamin A/C in C-ALCL should be characterized through a low to high level malignancy disease transformation.

Hypothesis

We hypothesized that the 3D telomere profiles, lamin A/C expression and lamin A/C structure would be altered in C-ALCL, with further alterations as C-ALCL evolved to an aggressive disease stage.

Aims

Aim 1a: To investigate the 3D nuclear organization of telomeres during a low-to-high level malignancy evolution of C-ALCL. I used three cell lines: Mac-1 isolated during a low-level malignancy state of C-ALCL to be compared with Mac-2A and Mac-2B, which were started at an aggressive state of C-ALCL of the same individual.
I aimed to quantify telomeric data including individual telomere lengths, count of telomere signals, count of telomere aggregates and *a/c* ratio (representing spatial distribution of telomeres) of individual cells using 3D telomere-FISH.
Aim 1b: To validate results, I also aimed to investigate telomere profiles of tissue samples from 3 other patients with an aggressive C-ALCL, one lymph node (JS10), one skin lesion (89Margie) and one breast implant associated (LS21) tissue.

Aim 2a-b: To investigate the expression and structure of lamin A/C protein in early and late-stage aggressive C-ALCL. I used the cell lines and tissue samples outlined in Aim 1 to complete this 2nd Aim. I aimed to quantify lamin A/C expression of individual cells and investigate whether any abnormal internal lamin A/C structures exist in this disease like those observed in HL (Contu *et al.,* 2018).

Materials and Methods

Figure 1. Workflow Diagram

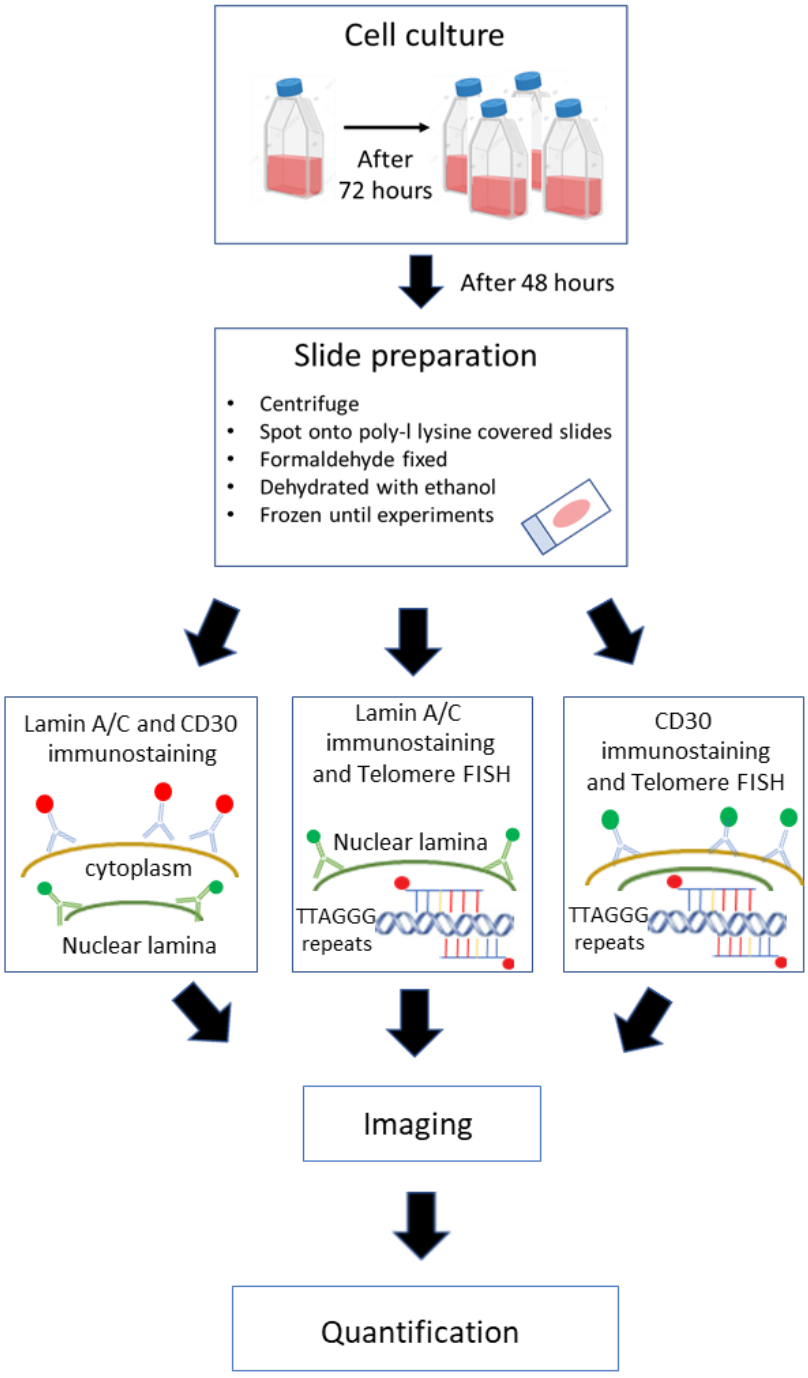

Cell Lines

Three cutaneous T-cell lymphoma cell lines, first described in Davis *et al.*, 1992, were used for this project: Mac-1 was started from circulating "Sézary-like" cells (atypically large) in peripheral blood, Mac-2A and Mac-2B were started from separate skin-tumor nodules of the

same patient that progressed to malignant C-ALCL (frozen samples supplied by Dr. Marshall Kadin, Brown University, Providence, RI 02912, United States, Davis *et al.*, 1992). All cells were grown in RPMI-1640 medium, supplemented with 20% fetal bovine serum (FBS), 1% L-glutamine, 1% sodium pyruvate, and 1% penicillin–streptomycin (all from Invitrogen, Burlington, ON, Canada). Cells were incubated at 37°C with 5% CO_2 in a humidified atmosphere. The cells were cultured in Nunc™ EasyFlask™ 75cm^2 (Thermo Scientific, Roskilde, Denmark).

Preparation of slides

Cells were passaged once, from 1 flask to 4 flasks, 72 hours after thawing. After another 48 hours, cells were prepared for experiments by spreading them onto poly-L-lysine (SIGMA, p8920, St. Louis, MO, USA) coated slides (O. Kindler GmBH, Ziegelhofstraße 214, 79110 Freiburg, Germany). Slides were fixed in 3.7 % formaldehyde/1× phosphate buffered saline (PBS) for 10 min at room temperature. Slides were then washed in 1 × PBS, shaking at room temperature, 3 times × 5 min. Slides were then dehydrated in series of 70, 90, 100% ethanol in H_2O, 3 min each, and then kept frozen at -20 °C until experiments.

Before the start of experiments, the slides were taken from the freezer and rehydrated in decreasing EtOH concentrations from 100% EtOH to 50% EtOH/H_2O.

Table 1. Antibodies used in immunostaining methods

Antibody targets	Concentration	Type-Source
Primary Lamin A/C	1:100	rabbit polyclonal, ab26300, Abcam Ltd., Cambridge, UK
Secondary Lamin A/C	1:500	Anti-rabbit antibody conjugated with the Alexa 488 fluorophore A-11008, Molecular Probes, Waltham, MA, USA
Primary CD30	1:100	Primary CD30 Antibody (Ber-H2) Mouse Monoclonal, MA5-13219, Thermo Fisher Scientific, Waltham, MA, USA
Secondary CD30	1:500	Anti-mouse antibody conjugated with the Cy3 fluorophore Polyclonal, AC111C, Merck & Co., Kenilworth, New Jersey, USA

Antibodies

Antibodies used for experiments were : 1) Primary Anti-Lamin A/C antibody (rabbit polyclonal, ab26300, Abcam Ltd., Cambridge, UK); 2) Secondary goat Anti-rabbit antibody conjugated with the Alexa 488 fluorophore (A-11008, Molecular Probes, Waltham, MA, USA); 3) Primary CD30 Antibody (Ber-H2) (Mouse Monoclonal, MA5-13219, Thermo Fisher Scientific, Waltham, MA, USA); 4) Secondary sheep Anti-mouse antibody conjugated with the Cy3 fluorophore (Polyclonal, AC111C, Merck & Co., Kenilworth, New Jersey, United States).

Co Immunostaining for lamin A/C and CD30

Slides were first incubated in 4% Bovine Serum Albumin (BSA)/4× saline-sodium citrate (SSC) blocking solution for 5 minutes at 37°C. A dilution of 1:100 for the primary antibodies and 1:500 for the secondary antibodies in 4%BSA/4×SSC blocking solution was used. Slides were incubated with both primary antibodies overnight at 37°C in humidified atmosphere and washed three times in 1xPBS, 5 min each. Incubation with secondary antibodies was performed for 1

hour at 37°C in humidified atmosphere and then washed three times in 1xPBS, 5 min each. DNA of the nuclei was counterstained with 1 ug/mL 4′,6-diamidino-2-phenylindole (DAPI) for 5 min. Slides incubated without primary antibodies (4%BSA/4×SSC blocking solution only) were processed in parallel as negative control. A drop of mounting medium Vectashield (Vector Laboratories Inc, Burlingame, CA, USA) was added to prevent photo bleaching before imaging.

Immunostaining for lamin A/C and Telo-Q-FISH

Immunostaining and Telo-Q-FISH protocol used here was adapted from a previously described protocol (Knecht and Mai, 2017). Q-FISH was performed by applying Cy3-Labeled peptide nucleic acid (PNA)-telomere probe (Dako, Glostrup, Denmark) in the dark, followed by a cycle of denaturation for 3 min at 80°C followed by hybridization for 2 h at 30°C using the HybriteTM (Vysis/Abbott, Abbott Laboratories. Abbott Park, Illinois, USA). The slides were then washed in 70% formamide/10 mM 2 times, 15 minutes each and then washed in 0.1× SSC at 55°C for 5 minutes. Two more washes in 2× SSC/0.05% Tween 20 were performed for 5 minutes each. Slides were then incubated in 4%BSA/4×SSC blocking solution for 5 minutes at 37°C before immunostaining. A dilution of 1:100 for the primary Anti-amin A/C antibody (rabbit polyclonal, ab26300, Abcam Ltd., Cambridge) and Secondary goat Anti-rabbit antibody conjugated with the Alexa 488 fluorophore (Molecular Probes, Waltham, MA, USA) was used. Slides were incubated with primary antibody overnight at 37°C in 4%BSA/4×SSC humidified atmosphere. Slides were washed three times in 1xPBS, 5 min each. Incubation with secondary antibody was performed for 1 hour at 37°C in humidified atmosphere, then slides were washed three times in 1xPBS, 5 min each. DNA of the nuclei was counterstained with 1 ug/mL DAPI for 5 min. Slides incubated without primary lamin A/C antibody (4%BSA/4×SSC blocking solution only) and no telomere probe were processed in parallel as negative control. A drop of mounting medium Vectashield (Vector Laboratories Inc, Burlingame, CA, USA) was added to prevent photo bleaching before imaging.

Immunostaining for CD30 and Telo-Q-FISH

CD30 and Telo-Q-FISH experiments were performed exactly as described above in "Immunostaining for lamin A/C and Telo-Q-FISH", substituting antibodies with primary CD30 Antibody (Ber-H2) (Mouse Monoclonal, MA5-13219, Thermo Fisher Scientific, Waltham, MA, USA) and secondary Alexa Fluor 488 antibody (Goat anti-Mouse IgG (H+L), AB_2534088, Thermo Fisher Scientific, Waltham, MA, USA)

3D Image acquisition

3D image acquisition was performed on 100 cells of each cell line, per experiment. Thirty multinucleated cells of Mac2a and Mac2b lines were image per experiment. The 3D imaging was performed using ZEISS Axio Imager.Z2 (Carl Zeiss, Toronto, ON, Canada) with a cooled AxioCam FITC, Cy3 and DAPI filters in combination with a Planapo 63x/1.4 oil objective lens (Carl Zeiss, Toronto, ON, Canada). Light microscopy images have an optical resolution at 102nm in x-y directions and 200 nm in z, accordingly, 60 z-stacks at 200nm step-size were imaged for every fluorophore. A FITC filter was used to visualize lamin A/C stain with a 300 ms exposure time. In "Co Immunostaining for lamin A/C and CD30" experiments, CD30 stain was also visualized with FITC filter and 300 ms exposure time. A Cy3 filter was used to visualize telomere probe with 800 ms exposure time. In "Co Immunostaining for lamin A/C and CD30" experiments, lamin A/C staining was also visualized with Cy3 filter using 500 ms exposure time per image. A DAPI filter was used to visualize the DNA with 8 ms exposure time in all experiments. Images were obtained using Zen Blue 3.1 (Carl Zeiss, Toronto, ON, Canada), deconvolved using the constrained iterative algorithm with Theoretical Point Spread Function and Clip Normalization (Schaefer *et al.,* 2001).

Quantitative analysis of lamin A/C and CD30 expression

Lamin A/C expression was analyzed on ZEN Blue Version 3.1 Software (Carl Zeiss, Jena, Germany). Lamin A/C structure appeared as a ring at nuclear periphery of cells; a single representative z-stack, where lamin A/C ring was widest, was selected for each cell. For lamin A/C quantification, analysis was done according to the methods of Contu *et al.,* 2018: Briefly, the "draw spline contour" tool was used to define two areas in the selected z-stack, the external

area and the internal area. The external area was defined as the part of the image where lamin A/C structure was visible (represented in red, Fig 2). The internal area is the part of the image with the nucleus but absent of lamin A/C structure (represented in blue, Fig 2). The external lamin A/C intensity (Ie) was the total signal intensity within defined external area, while the internal total lamin A/C intensity (Ii) was the total signal intensity within the internal area. An intensity ratio (Ie/Ii) was calculated dividing Ie by Ii to normalize the signal with cell area. For quantifying CD30 expression, the "draw spline contour" tool was used to draw a zone enclosing the visible CD30; the signal sum was divided by area to generate a final number.

Figure 2. Lamin A/C and CD30 quantification

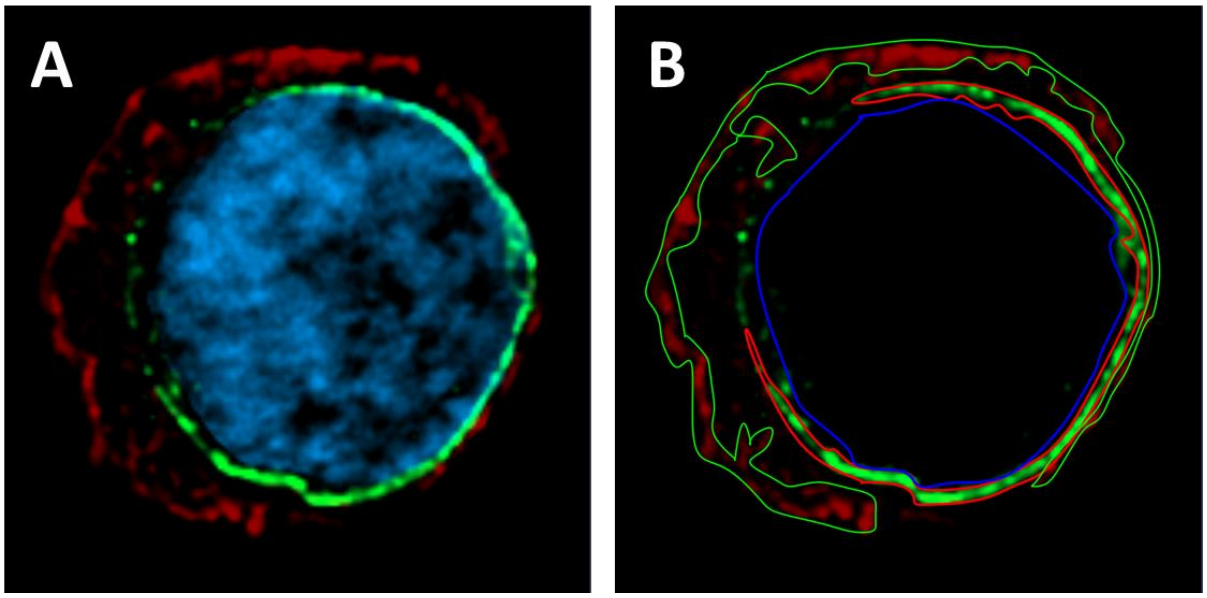

A) Image of a Mac-2a cell. CD30 staining in red, lamin A/C staining in green, DAPI DNA stain in blue. B) The external total lamin A/C intensity (Ie) was the total signal sum from the area enclosed with red. The internal total lamin A/C intensity (Ii) signal was the sum of the area enclosed in blue. The final number representing lamin A/C expression of a cell was Ie/Ii. CD30 expression was quantified as the signal sum of the area enclosed in green divided by its area.

Telomere analysis

Deconvolved images were converted into TIFF files and exported for 3D analysis using the TeloView software (version 2.0, Telo Genomics, Toronto, ON, Canada) (Vermolen *et al.*, 2005). The following data points were generated by TeloView software, per cell, and used in this study: 1) Count of telomere signals, 2) Count of telomere aggregates, 3) Signal intensity of each telomere, which is indicative of telomere length, and 4) count of telomere aggregates. Telomere aggregates are defined as telomeres clustered in a proximity of less than 200 nm, a distance that cannot be resolved as separate entities by conventional light microscopy.

Statistical analysis

Statistical analysis was done using R version 4.1.1 and Rstudio version 1.4.1717 (R Core Team, 2021; Rstudio Team, 2021). Telomere data, lamin A/C expression and CD30 expression were analyzed by Kruskal–Wallis one-way analysis of variance. Upon significance of $p \leq 0.05$, data was further analyzed in group pairs with Wilcoxon signed-rank test with Bonferroni correction.

Results

I have compared the nuclear organization of 3 C-ALCL cell lines of the same clonal origin but differing disease stages to gain insights into the nuclear remodelling that takes place during evolution of this cancer. I have also compared three tissue samples of different C-ALCL backgrounds to establish a baseline for heterogeneity of their nuclear organization and to look for any significant differences that are attributable to their origins. The origins of these three cell lines and tissue samples, respectively, and their relations between each other have been summarized in Table 2.

Table 2. Origins of diverse C-ALCL cancer cell lines and tissue samples I examined in my study

Cell lines	Source	Disease	References
Shared clonal origin: Mac-1	Circulating Sézary-like cells in the peripheral blood, 1985	lymphomatoid papulosis of histologic type A (benign)	Davis et al., 1992
Shared clonal origin: Mac-2A, Mac-2B	From separate ulcerating skin lesions ,1987 same day	CD30+ cutaneous anaplastic large-cell lymphoma (malignant)	Davis et al., 1992
Tissue samples			
JS10	Lymph node	CD30+ cutaneous anaplastic large-cell lymphoma (malignant)	Csikesz et al., 2013
LS21	Biopsy around breast implant	CD30+ Breast Implant Associated Lymphoma (BIA-ALCL)	Not published
Margie89	Skin tumor nodule	CD30+ cutaneous anaplastic large-cell lymphoma (malignant)	Volkenandt et al., 1993

In this study, multiple significant differences in-between cell lines and between the tissue samples investigated have been detected. In HL, telomere remodelling is associated with transition of mono nucleated H cells to RS cells, while an aberrantly placed overexpression of lamin A/C is both associated with and found to be necessary for this transition (Knecht *et al.*, 2009; Contu *et al.*, 2018). The existence of RS -ike multinucleated cells in Mac cell lines has led us to question whether similar trends could be observed in C-ALCL. I also compared the multinucleated subpopulations to mononucleated cells of the same cell line. All statistically significant findings are briefly summarized in Table 3. All individual findings are then detailed in figures and subsections below.

Table 3. Summary of all significant differences our analysis detected between cell lines, subpopulations of cell lines and tissue samples

Data	Cell lines results	Multinucleated	Tissues
Telomere counts per nuclei or nuclei fragments for tissue (levels of aneuploidy)	Mac-1 cells have significantly fewer telomeres compared to Mac-2A and Mac-2B cells (Mac-1< Mac-2=Mac-2B)	Multinucleated Mac-2A and Mac-2B cells have more telomeres compared to their mononucleated counterparts	CD30 positive cell segments from 89Margie and JS10 have more telomeres compared to LS21
Average telomere lengths	Mac-1 cells have the longest telomeres, followed by Mac-2B. Mac-2A telomeres are shortest (Mac-1>Mac2B>Mac2A)	Multinucleated Mac-2A have longer telomeres compared to other Mac-2A cells while multinucleated Mac-2B cells have shorter telomeres compared to their counterparts	CD30 positive cell segments from LS21 and 89Margie have longer telomeres compared to JS10
Spatial organization of telomeres	Mac-1 and Mac-2B telomeres are distributed in a more spherical 3D organization. Mac-2A telomeres are organized in a more flatter disc-like 3D distribution	Multinucleated Mac-2B and Mac-2A telomeres are organized in a flatter 3D volume compared to mononucleated Mac-2B cells	
Lamin A/C expression of cells or cell fragments	Mac-2A has the greatest lamin A/C expression followed by Mac-1. Mac-2B has the weakest and often no expression. (Mac-2A>Mac-1>Mac-2B)	Multinucleated Mac-2B cells have greater Lamin A/C expression compared to other Mac-2B cells	Only a few CD30 positive cell segments are lamin A/C positive. Expression is generally too weak to quantify
CD30 expression of cells or cell fragments	Mac-1 cells have significantly lesser CD30 expression compared to Mac-2A and Mac-2B (Mac-1<Mac-2A=Mac-2B)	Multinucleated Mac-2B cells have weaker CD30 expression	

3D nuclear organization of telomeres in Cutaneous Anaplastic Large Cell Lymphoma derived cell lines

I performed three-dimensional analysis of telomere profiles using quantitative fluorescent *in situ* hybridization (Q-FISH) which revealed differences between the benign C-ALCL parent line and derived malignant lines and also differences between the two malignant lines Mac-2A and Mac-2B (Fig. 3A-E). Figure 3 A and B are representative 2D and 3D images of telomere organization in Mac cells. Telomere counts per cell indicated no significant differences of aneuploidy between Mac-2A and Mac-2B, but there was a significant difference compared to their parent cell line, Mac-1, which had fewer telomere signals ($p = 0.00046$ compared to Mac-2A, $p= 0.00061$ compared to Mac-2B. Fig.3C). Results of interphase Q-FISH here are in line with previous observations from metaphase Giemsa staining that reported Mac-2A and Mac-2B cells having numerous additional chromosomal abnormalities compared to Mac-1 (Davis *et al.,* 1992). I observed an average of 40 telomeric signals for Mac-1 and 48 for Mac-2A, Mac-2B. It is theoretically expected to see 92 telomeres in normal human cells; however, due to resolution limit of conventional microscopy, telomeres that are in closer proximity than 200 nm cannot be resolved. In my experimental setting, telomere counts of 25-55 per cell appeared to be normal, which was in line with previous findings using similar protocols (Fig.3; de Vos *et al.,* 2009; Knecht *et al.,* 2013; Mathur *et al.,* 2014).

Figure 3D shows a graphical view of the intensity of each telomere observation of the three cell lines. In telomere lengths, benign cell line Mac-1 had the longest telomeres (Mac-1 longer than Mac-2A; $p < 10^{-6}$, Mac-1 longer than Mac-2B; $p = 2.5 \times 10^{-5}$); however Mac-2B telomeres also showed a small but significant increase in length compared to Mac-2A telomeres (Mac-2B longer than Mac-2A $p = 1.33 \times 10^{-4}$, Fig.3D).

11-12% of telomeric signals in Mac cell lines were identified as telomere aggregates. There is no difference related to the frequency of aggregates between cell lines.

Finally, telomere profiles differed between the three cell lines in terms of their 3D spatial distribution. Mac-2A telomeres were arranged closer to a flatter disc-like 3D distribution, while Mac-1 telomeres were more spherical in their 3D distribution (Fig. 3E, $p < 10^{-6}$). Mac-2B telomeres occupied an even more spherical 3D volume (Fig. 3E, Mac-1 vs Mac-2B; $p= 2.71 \times 10^{-4}$, Mac-2A vs. Mac-2B; $p < 10^{-6}$).

Figure 3. 3D nuclear organization of telomeres in Mac cell lines

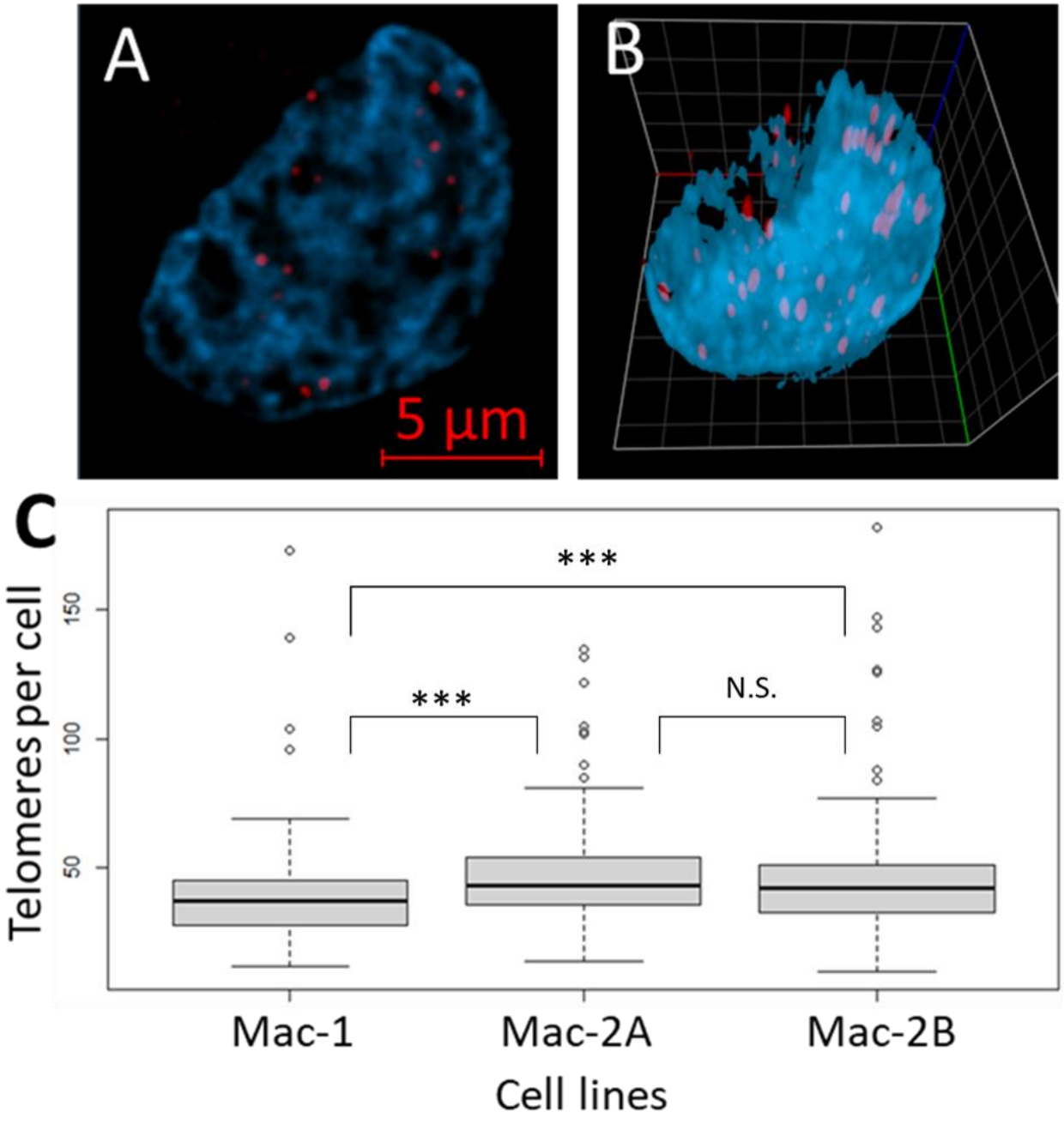

D

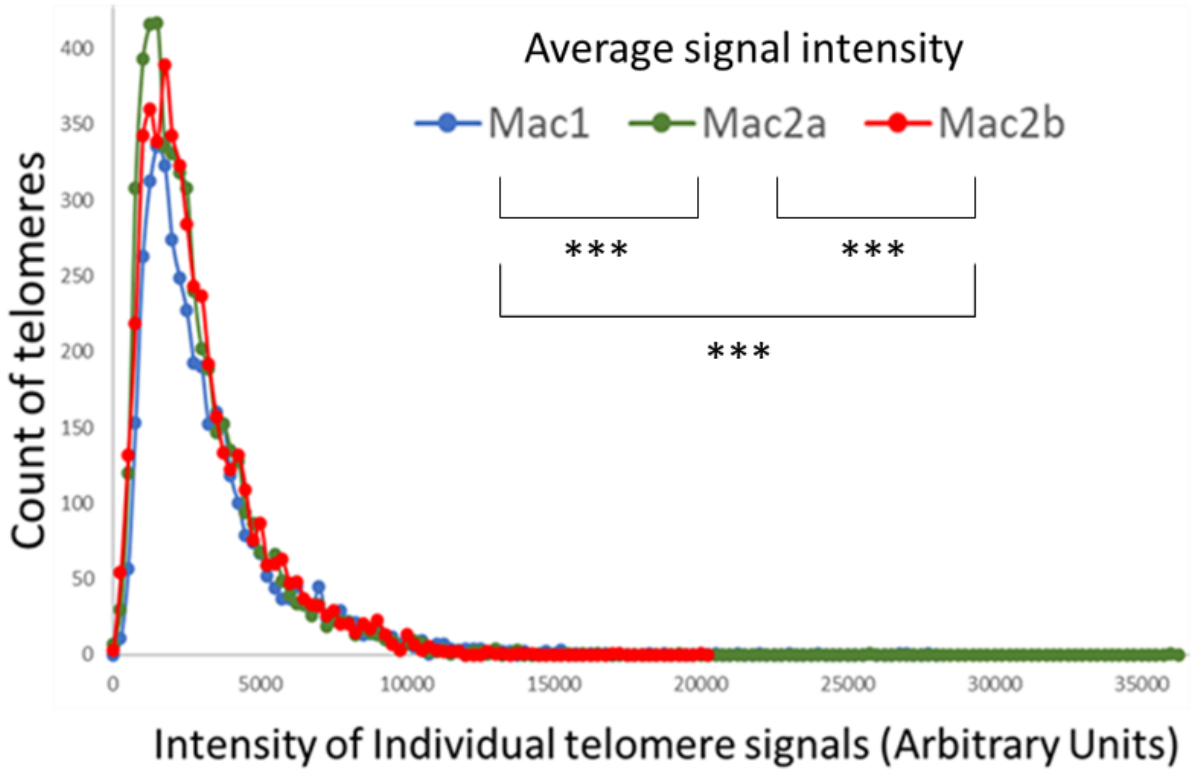
Average signal intensity
Mac1
Mac2a
Mac2b
***
***
***
Count of telomeres
400
350
300
250
200
150
100
50
0
0
5000
10000
15000
20000
25000
30000
35000
Intensity of Individual telomere signals (Arbitrary Units)

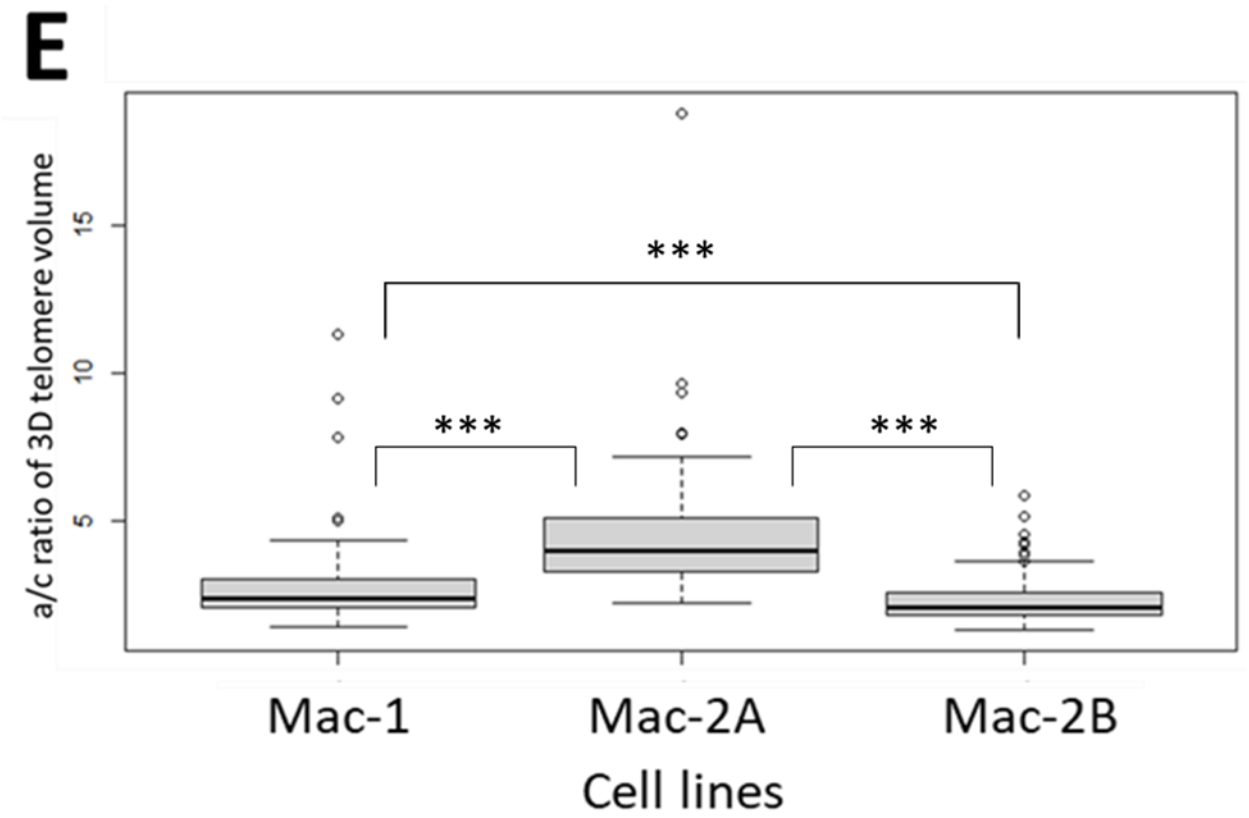

(A) A representative 2D image chosen from Z-stack of a Mac-2B cell, telomere signal in red and DAPI DNA stain in blue. **(B)** 3D view of the same cell, representative of 3D telomere organization appearance in all cell lines. **(C)** Boxplot of telomere counts per cell. For Mac-1, about 40 telomeres were detected per cell on average. For Mac-2A and Mac-2B, an average of about 48 telomeres were detected per cell which was significantly more compared to Mac-1 ($p = 4.60 \times 10^{-4}$, $p = 6.10 \times 10^{-4}$, respectively). A total of 103 cells were analyzed per cell line. **(D)** Signal intensity distribution of all telomeres from the three cell lines. A total of 4100 telomeres were detected for Mac-1, 4985 telomeres for Mac-2A and 4896 telomeres for Mac-2B. For Mac-1, I determined an average signal intensity of 3276 AU (Arbitrary Unit), for Mac-2A average telomere intensity was 2902 AU which indicates significantly shorter telomeres compared to Mac-1 ($p < 10^{-6}$). Mac-2B telomeres were detected to have an average intensity of 3010 AU, significantly shorter than Mac-1 ($p = 2.5 \times 10^{-5}$) but also significantly longer than Mac-2A ($p = 3.24 \times 10^{-4}$) **(E)** Boxplot of nuclear *a/c* ratios, which is a quantitative measure of 3D telomere spatial positioning, between the three cell lines. Comparison indicates a higher *a/c* ratio for Mac-2A telomeres suggesting that they are organized in a flatter 3D volume compared to a more

spherical 3D distribution of Mac-1 telomeres. Mac-2B telomeres are organized in an even more spherical way (Mac-1 vs. Mac-2A; $p < 10^{-6}$, Mac-1 vs Mac-2B; $p= 2.71 \times 10^{-4}$, Mac-2A vs. Mac-2B; $p < 10^{-6}$).

Lamin A/C expression patterns in Cutaneous Anaplastic Large Cell Lymphoma derived cell lines

To determine patterns of lamin A/C expression in C-ALCL cell lines, I performed immunostaining. All cell lines showed staining of lamin A/C, unlike normal T cells which they are derived from (Fig.4). Figure 4 A-D are representative 2D images of variation of lamin A/C expression. For Mac-2A, all cells were observed to express lamin A/C which appeared as a ring structure around the nuclei (Fig.4 A-B). For Mac-1 and Mac-2B it was possible to find cells that did not express lamin A/C (Mac-2B cells in Fig.4 C-D). Figure 4 E-F show 3D images that are representative of the lamin A/C structure of all cells that had visible lamin A/C expression. Lamin A/C was found to form a uniform ring shape in images restricted to the nuclear periphery.

Mac-2A cells expressed the highest amount of lamin A/C among the three cell lines and all Mac-2A cells are found to have detectable lamin A/C expression (Fig 4A-B, Fig 5). This contrasts with Mac-2B, another C-ALCL cell line that originates from the same disease stage (collected on the same day), which had the weakest lamin A/C expression ($p < 10^{-6}$ compared to Mac-2A and $p < 10^{-6}$ compared to Mac-1 as well, Fig.5), with 24-25% of cells having no lamin A/C expression by immunostaining. Mac-1, the parent cell line, expressed lamin A/C to a lesser extent compared to Mac-2A ($p = 3.99 \times 10^{-4}$, Fig 5) but more than Mac-2B. Less than 10% of the Mac-1 cells were negative for lamin A/C immunoreactive protein.

Figure 4. Lamin A/C protein staining in C-ALCL cell lines

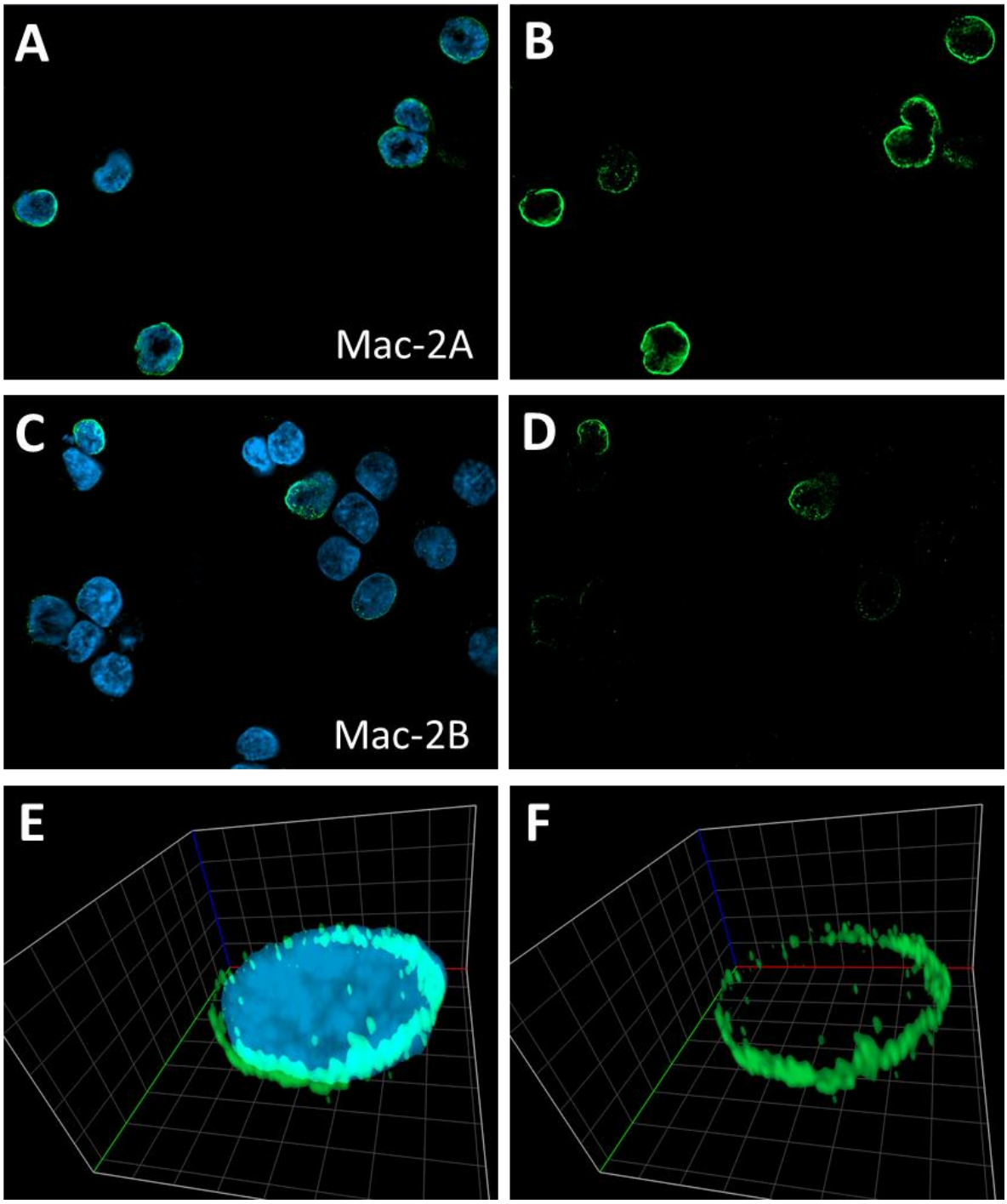

(A) 2D representative image of Mac-2A cells with lamin A/C immunostaining in green and DAPI DNA staining in blue. **(B)** Same 2D image as **A**, with only lamin A/C channel active. All cells expressed lamin A/C in ring shaped pattern at the nuclear periphery. **(C)** 2D image

representative of both Mac-2B and Mac-1 not expressing immunoreactive lamin A/C. Image shown with identical exposure settings compared to **A** and **B (D).** Same 2D image as **C**, with only lamin A/C channel displayed. Weakness of the fluorescent signal is indicative of weaker lamin A/C expression. Some cells have no visible lamin A/C. **(E-F)** 3D representative images of lamin A/C pattern in Mac cells. Image shows a Mac-2A cell where lamin A/C is uniformly immunostained at the nuclear periphery. Exposure time for lamin A/C was 300 ms per z-stack in all images.

Figure 5. Boxplot of lamin A/C expression quantifications

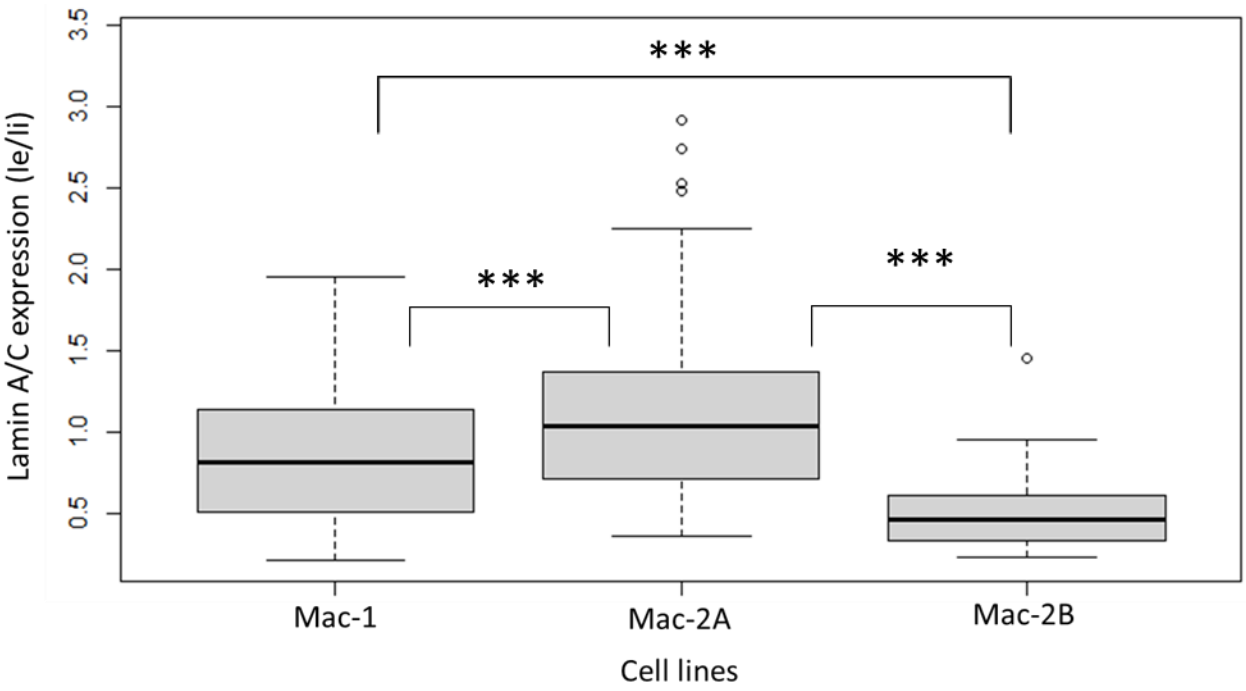

Fig 5. 100 cells per cell line were analyzed and grouped for comparison. Mac-2A cells have the highest lamin A/C expression; ($p = 4.0 \times 10^{-4}$ compared to Mac-1, $p < 10^{-6}$ compared to Mac-2B). Mac-1 cells have higher expression compared to Mac-2B ($p < 10^{-6}$)

Multinucleated Mac cells

In line with previous observations, I observed atypical large cells; these resembled HL Reed-Sternberg (RS) cells or Sézary cells of CTCL (Davis *et al.*, 1992, Fig 6.). These cells made up <1% of Mac-1 but were more prominent at about 10% in Mac-2A and Mac-2B. Previous publications have not noted that these large cells can be mononucleated, unlike the RS cells they resembled. There were also smaller lymphocyte-sized Mac cells that were multinucleated, which have also not been reported before (Fig 6). Multinucleated cells were of particular interest as this subpopulation has accumulated further genome alterations. I focused further on multinucleated Mac cells as an important atypical group, including both lymphocyte-sized and large cells. Multinucleated cells again made up less than 1% of Mac-1 and some 10% of Mac-2A and Mac-2B, respectively.

I analyzed multinucleated cells to determine how their telomere profiles and lamin A/C expression differed from the majority of the mononucleated population of the same cell line. Mac-1 cell line did not have sufficient numbers of multinucleated cells to draw statistically significant conclusions.

Figure 6. Examples of atypical Mac cells

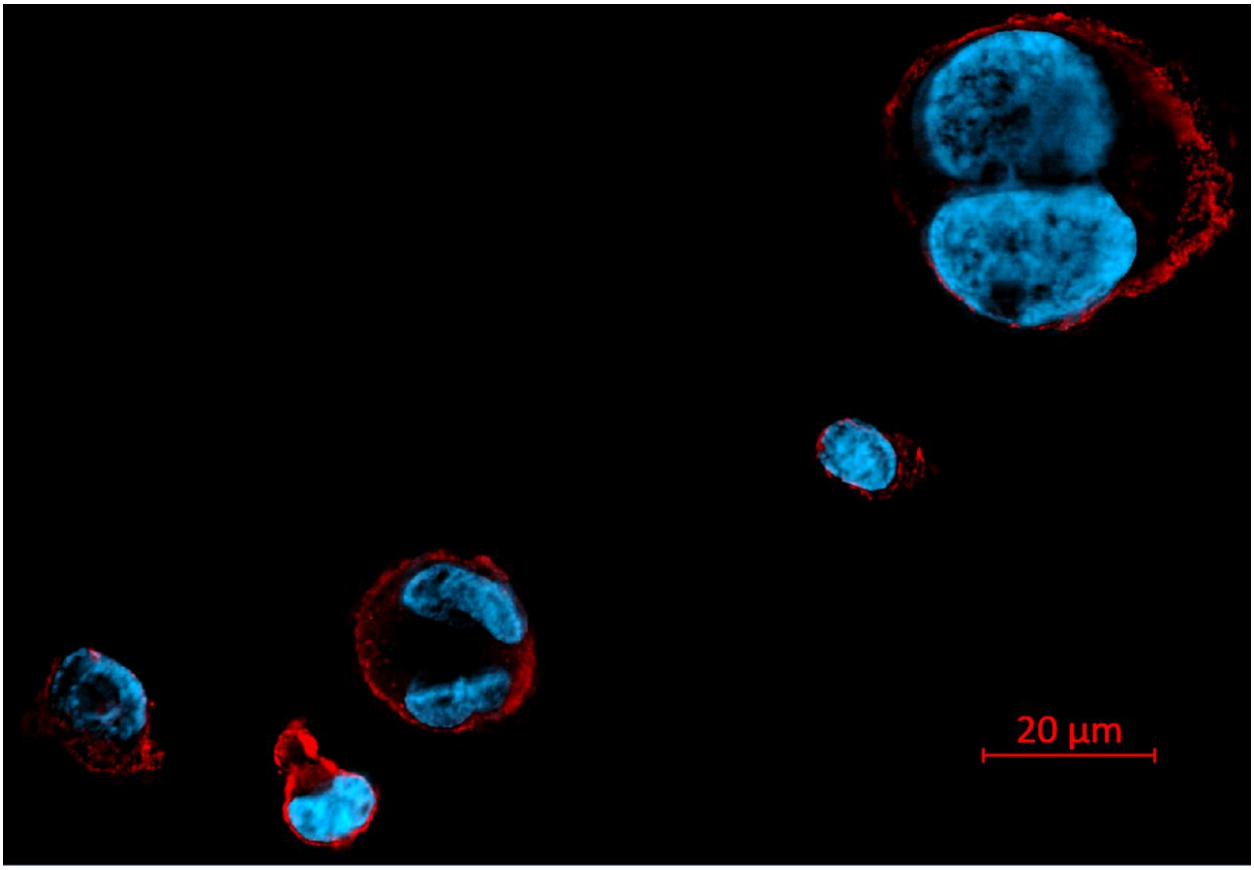

Fig 6. A 2D image from Mac-2A line is shown with CD 30 cell surface marker immunostaining in red and DAPI DNA staining in blue. Three typical mononucleated lymphocyte sized cells can be seen alongside two binucleated cells: one RS-like binuclear cell and a smaller binuclear cell.

Telomere profile differences of multinucleated Mac cells

Multinucleated cells had a higher telomere count compared to their mononucleated sisters (for Mac-2A $p < 10^{-6}$, for Mac-2B $p < 10^{-6}$). For Mac-2A, multinucleated cells had longer telomeres compared to mononucleated cells ($p=1 \times 10^{-6}$, Fig 7). For Mac-2B, the opposite was true; multinucleated cells had shorter telomeres compared to mononucleated Mac-2B cells ($p < 10^{-6}$, Fig 7). Telomere aggregates made up 11-12% of all telomeric signals in these cells and no differences were detected between multinucleated and mononucleated cells or between cell lines.

Spatial distribution of telomeres was found to be altered in a similar manner for both cell lines. The telomeres of multinucleated cells were arranged close to a flattened disc in 3D distribution, while mononucleated cells were arranged in a more spherical 3D distribution ($p = 0.054$ for Mac-2A, $p < 10^{-6}$ for Mac-2B, Fig 7)

Figure 7. Telomere profiles of multinucleated Mac cells compared to mononucleated Mac cells

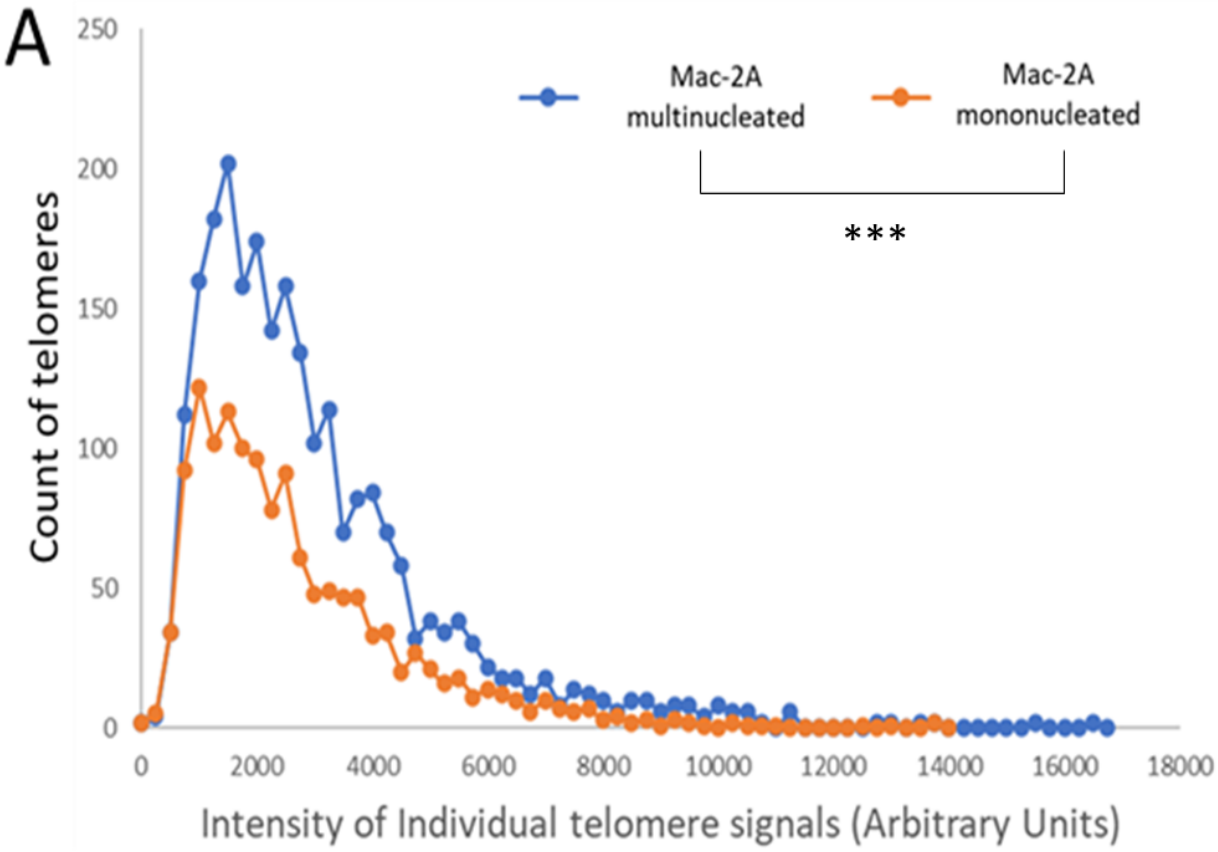

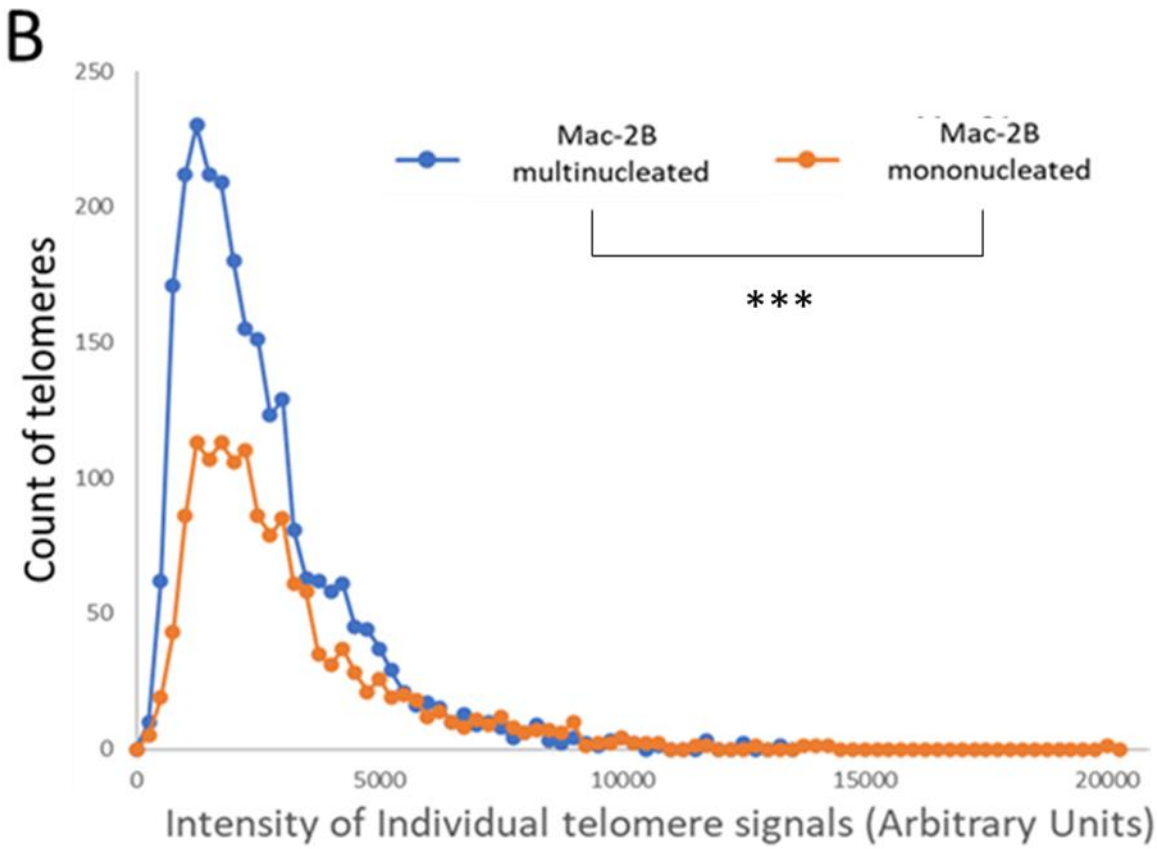
B
Mac-2B multinucleated
Mac-2B mononucleated
***
Count of telomeres
250
200
150
100
50
0
0
5000
10000
15000
20000
Intensity of Individual telomere signals (Arbitrary Units)

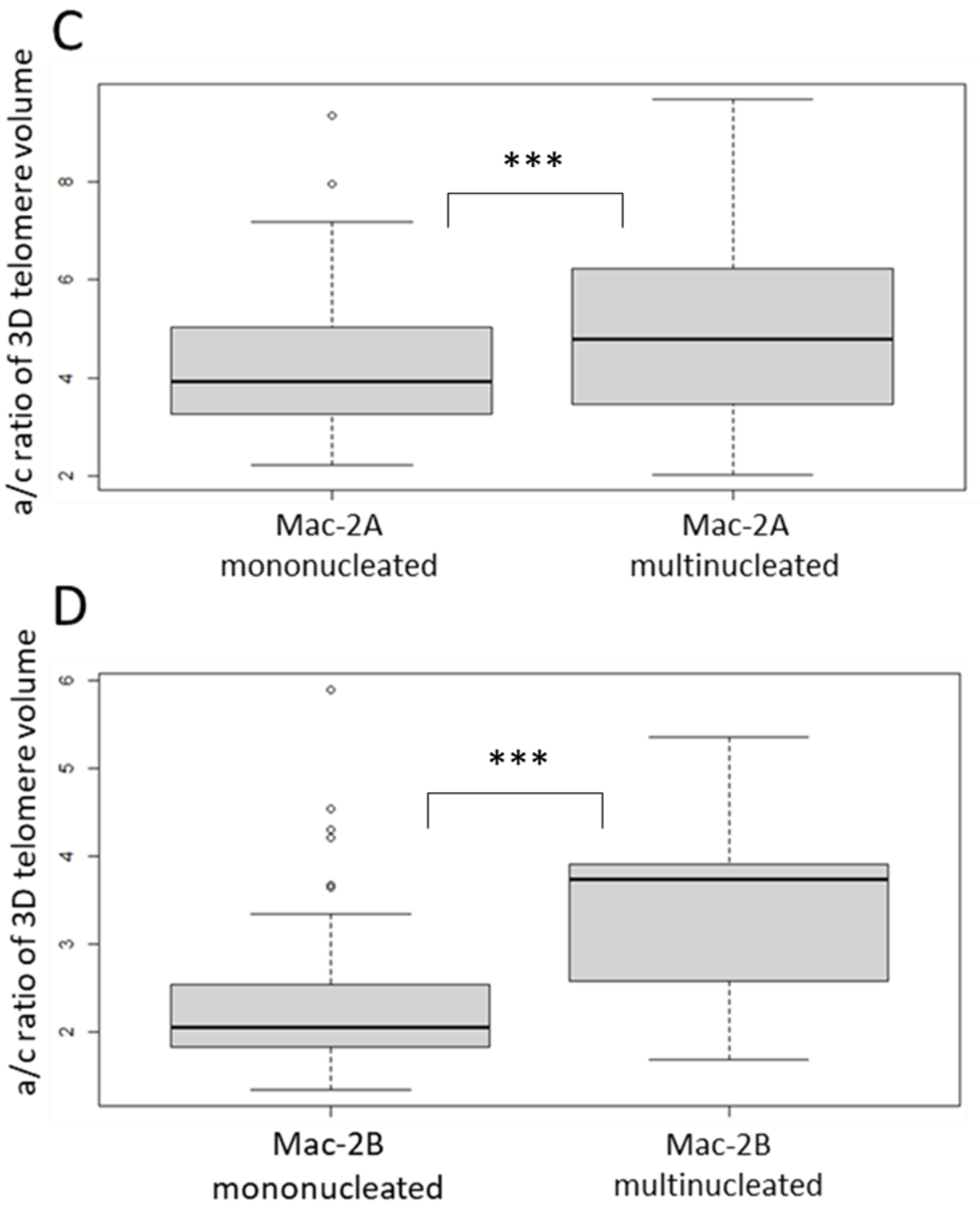

(A) Signal intensity distribution of all telomeres from Mac-2A multinucleated vs mononucleated cells. All telomeres from 30 mononucleated (N=1367 telomeres) and 30 multinucleated (N=2438 telomeres) cells were analyzed. Comparison of signal intensities showed multinucleated Mac-2A cells had longer telomeres compared to mononucleated Mac-2A cells ($p = 1 \times 10^{-6}$) Average

signal intensities were 3143 AU (Arbitrary Unit) for multinucleated cells and 2902 AU for mononucleated cells. **(B)** Signal intensity distribution of all telomeres from Mac-2B multinucleated vs mononucleated cells. All telomeres from 30 mononucleated (N=1609 telomeres) and 30 multinucleated (N=2766 telomeres) cells were analyzed. Comparing signal intensities showed multinucleated Mac-2B cells had shorter telomeres compared to mononucleated Mac-2B cells ($p < 10^{-6}$) Average signal intensities are 2653 AU for multinucleated cells and 3046 AU for mononucleated cells. **(C)** Boxplot of nuclear *a/c* ratios, which is a quantitative measure of 3D telomere spatial positioning, between multinucleated and mononucleated Mac-2A cells. 30 cells were analyzed for multinucleated cells and 100 cells were analyzed for mononucleated cells. Comparison indicated a difference where multinucleated telomeres were organized in a flatter 3D volume compared to mononucleated Mac-2A cells ($p = 0.0539$). **(D)** Boxplot of nuclear *a/c* ratios, which is a quantitative measure of 3D telomere spatial positioning, between multinucleated and mononucleated Mac-2B cells. 30 cells were analyzed for multinucleated cells and 100 cells were analyzed for mononucleated cells. Comparison showed a difference where multinucleated telomeres are organized in a flatter 3D volume compared to mononucleated Mac-2B cells ($p < 10^{-6}$)

Lamin A/C expression of multinucleated Mac cells

On average, multinucleated Mac-2A cells had less lamin A/C expression compared to their mononucleated sisters, but this difference is not significant at p=0.05 level (Fig 8, p=0.0752). Multinucleated Mac-2B cells, on the other hand, had lamin A/C upregulation ($p=3.30 p \times 10^{-4}$). Both groups showed a uniform nuclear distribution pattern that appeared ring-shaped in 3D deconvolved images. I did not observe internal lamin A/C structures and nuclear compartmentalization such as described in other lymphomas (Contu *et al.,* 2018).

Figure 8. Boxplot of lamin A/C expression quantifications with multinucleated cells of C-ALCL lines

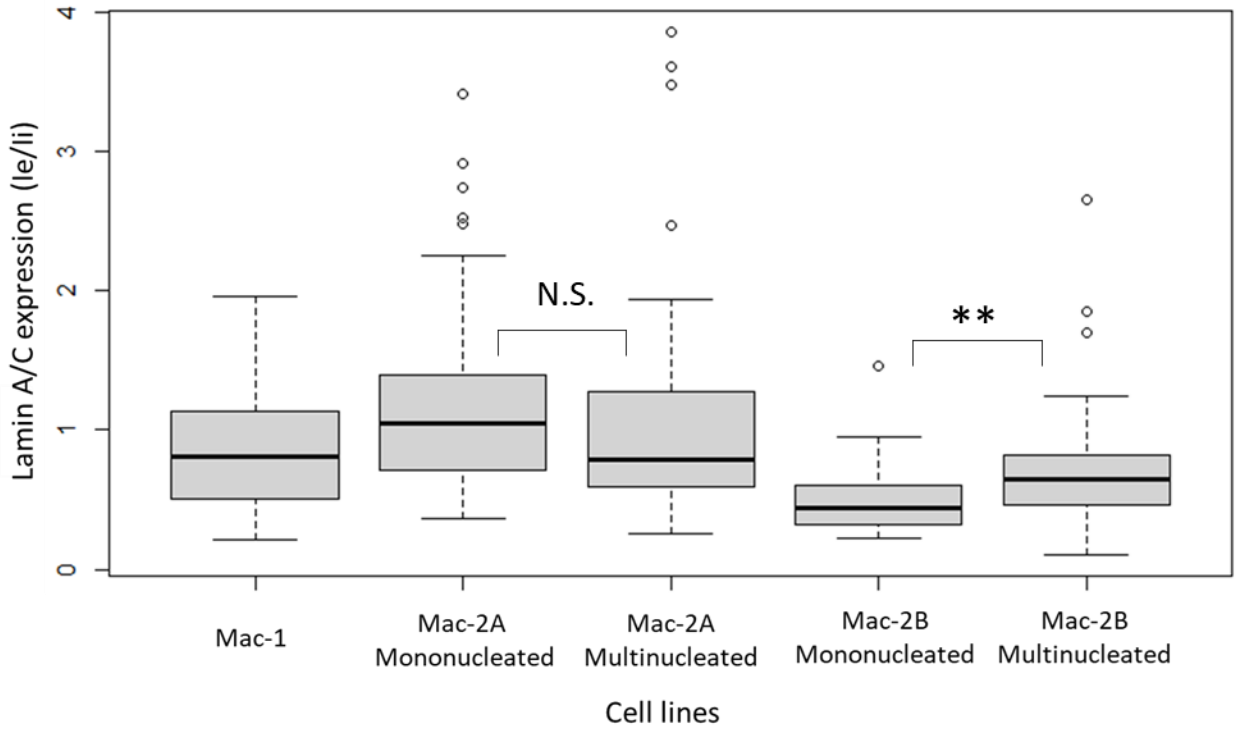

Fig 8. 100 cells were analyzed for each of Mac-1, Mac-2A mononucleated and Mac-2A mononucleated groups. Since multinucleated cells were rare, 30 cells were used in analysis of Mac-2A multinucleated and Mac-2B multinucleated groups. Our objective was to determine differences between multinucleated and mononucleated cells. Mac-2A multinucleated cells did not significantly differ from Mac-2A mononucleated cells in expression at p= 0.05 (p=0.0753) but show a trend where they express less lamin A/C. Mac-2B multinucleated cells significantly expressed more lamin A/C compared to mono nucleated Mac-2B cells (p= 0.00333).

Telomere lengths and counts differ between C-ALCL cells from tissue samples of different sources

Telomere profiles from the 3 C-ALCL tissue samples showed some significant differences. In these experiments, due to existence of non-cancer cells in the tumor microenvironment, I relied on CD30 cancer cell surface marker positivity to identify ALCL cells. Since tissues were preserved in paraffin blocks and cut for experiments, here cells are generally termed as cell sections since they are often partially cut. I naturally detected fewer telomeric signals from cell sections: 21 telomeres on average per cell sections were detected for JS10, 19 telomere signals on average were detected for Margie89 cell sections and 10 telomeres on average for LS21 cell sections. LS21, which was from a Breast Implant Associated ALCL setting, had significantly fewer telomeres compared the other 2 lines (Fig 9C. $p = 0.00750$ compared to JS10, $p = 0.0386$ compared to Margie89).

Figure 9D shows intensities of telomeric signal as a function of telomere length and grouped by tissue sample. Here, I observed that JS10 telomeres, which were from lymph node infiltrating ALCL cells, were shorter compared to other samples (Fig 9D, $p = 4.5 \times 10^{-5}$ compared to LS21, $p = 2.73 \times 10^{-4}$ compared to Margie89).

Figure 9. 3D nuclear organization of telomeres in ALCL tissue samples

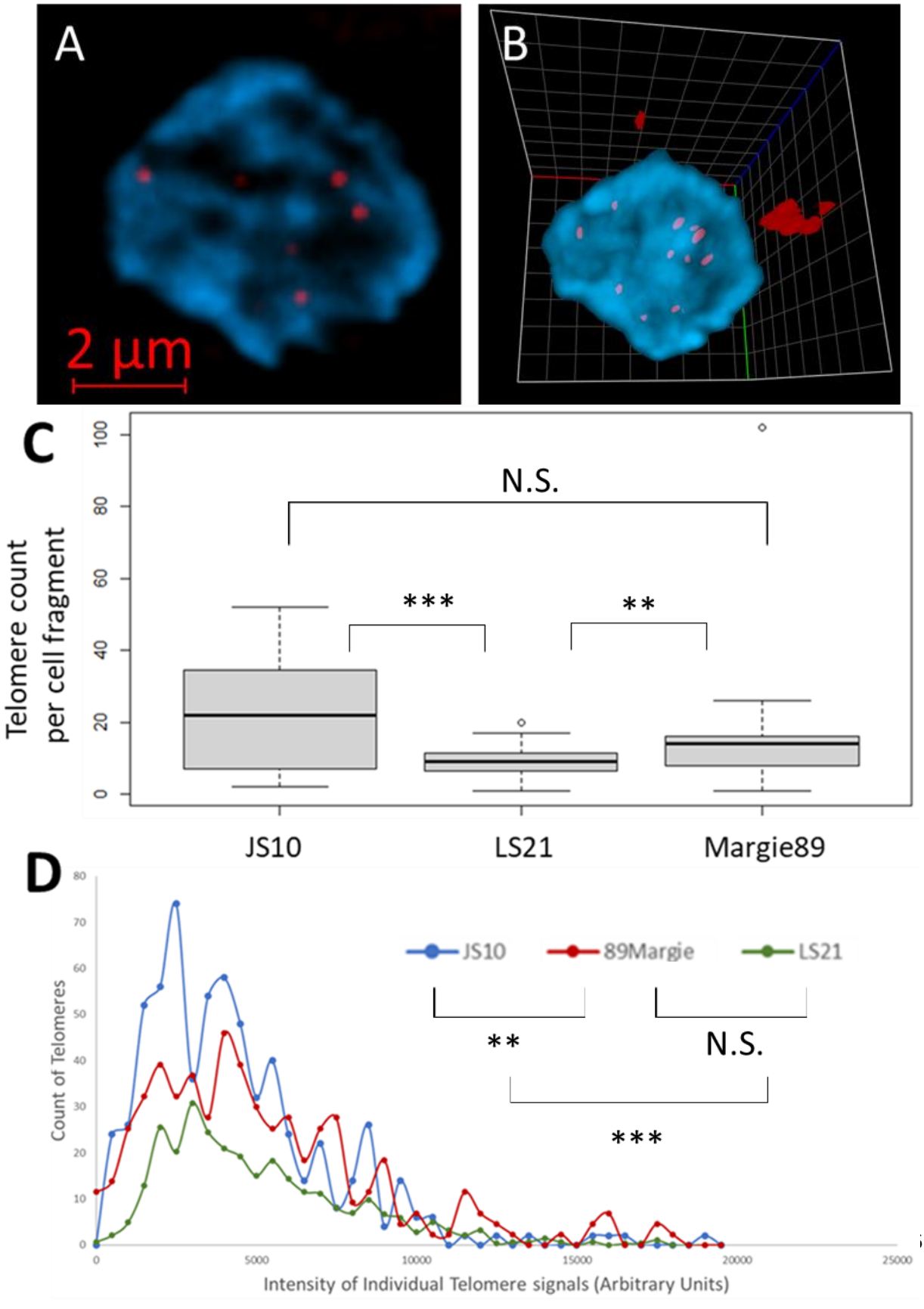

(A) A representative 2D image chosen from Z-stack of a LS21 cell segment, telomere signal in red and DAPI DNA stain in blue. **(B)** 3D view of the same cell segment, representative of 3D telomere organization appearance in all tissue samples. **(C)** Boxplot of telomere counts per cell segment. For JS10, about 21 telomeres were detected on average per cell sections. For Margie89, 19 telomeres were detected, not significantly different from JS10. LS21 cell sections had an average of 10 telomeric signals per cell section, which is significantly fewer than the other two. ($p = 4.5 \times 10^{-5}$ compared to JS10, $p = 0.00273$ compared to Margie89. A total of 30 cells were analyzed per tissue sample. **(D)** Signal intensity distribution of all telomeres from the 3 tissue samples. A total of 652 telomeres were detected for JS10, 572 telomeres for Margie89 and 291 telomeres for LS21. For JS10, I determined an average signal intensity of 4580 AU, indicating significantly shorter telomeres compared to LS21 which had an average signal of 5298 AU ($p = 4.5 \times 10^{-5}$). JS10 telomeres also had significantly shorter than Margie89 telomers which have an average signal of 5996 AU ($p = 0.002730$). No significant differences are detected between LS21 and Margie89.

Lamin A/C expression of C-ALCL cells in tissue samples is rare

I investigated immunoreactive lamin A/C expression in 150 cells per tissue. Cells that were both immunopositive for ALCL cell surface marker CD30 and lamin A/C were rare. Compared to other cells in the tumor microenvironment, CD30 positive cells were less likely to be immunopositive for lamin A/C (data not shown). Immunoreactive lamin A/C was too rare and weak to be quantitatively compared between tissue samples. When lamin A/C was observed, it still appeared as a ring structure around the nucleus.

Discussion

My project is the first to describe single cell 3D telomere profiles and lamin A/C expression in C-ALCL. This study generated first insights on how C-ALCL cells remodel their 3D genome by genomic instability during disease progression. This study identified significant differences between different C-ALCL cell lines and tissues. This has contributed to a better understanding of the baseline heterogeneity of C-ALCL nuclear organization.

The study of 3D nuclear organization alterations is an evolving field and has been a successful approach in characterizing various disease settings. Characteristic 3D telomere remodeling has been previously identified in acute myeloid leukemia (Gadji *et al.,* 2012), Hodgkin's Lymphoma (Guffei *et al.,* 2010), circulating tumor cells from various solid tumors (Adebayo Awe *et al.,* 2013) and importantly, in lamin A/C related laminopathies (Raz *et al.,* 2008), including Hutchinson-Gilford progeria syndrome (Mounkes & Stewart, 2004). These changes of 3D telomere profile can be of clinical significance and have diagnostic and/or prognostic value.

Previously, telomere lengths in C-ALCL had been assessed as a patient average and then compared with other CTCL patients and healthy volunteers (normal lymphocytes) (Chevret *et al.,* 2014). It was observed that C-ALCL cells on average had telomere lengths that were comparable to healthy lymphocytes, longer compared to other aggressive CTCL. This could be expected from cells that are slower in proliferation and have less replicative stress on their telomeres. Longer telomeres could also mean that C-ALCL has less genomic instability due to reduced rate of BFB cycles compared to other CTCL. C-ALCL could therefore be slower to acquire aggressive traits and have less heterogeneity to resist treatment. This phenotype is attributable to C-ALCL generally having a good prognosis compared to other CTCL. However, no C-ALCL data on single cell telomere lengths or to any extent data on telomere counts, 3D spatial telomere distribution, existence of telomere aggregates had been reported to date.

Collectively terming these parameters "3D telomere profiles", an aim of my project was to describe how the 3D telomere profile changes during C-ALCL evolution. I performed telomere Q-FISH experiments to achieve this goal. As stated above, C-ALCL is generally not highly malignant; however, I compared a low-level malignant stage of the disease, represented

by Mac-1, with an advanced malignant stage that transformed from the early state and accumulated enough changes that ultimately led to the patients' death, represented by Mac-2A and Mac-2B. Here, I found that telomere lengths get shorter through such a transformation when comparing Mac-1 to Mac-2A and Mac-2B (Fig. 3, $p < 0.05$). This erosion is an aspect of C-ALCL telomere profile that gets phenotypically closer to other malignant CTCLs and deviates from healthy lymphocytes as C-ALCL becomes aggressive.

Advanced malignant stages also had more telomeres (Fig. 3, $p < 0.05$). Mac-2A and Mac-2B had been reported (Davis *et al.,* 1992) to have "Numerous additional chromosomal abnormalities (compared to Mac-1)" in metaphase spreads in the first study of these cell lines. Our quantitative analysis revealed that these C-ALCL lines showed increased aneuploidy through cancer evolution with a net gain of chromosomes. Variations in aneuploidy became more prevalent as evident by the emergence of multinucleated and RS-like cells in later disease stage. Differences of multinucleated cells are discussed in their own segments with detail below. As expected, multinucleated cells had more telomeres compared to their mononucleated sisters. Existence of telomere aggregates, indicative of ongoing BFB cycles commonly in cancer cells but not detected in healthy cells (Mai & Garini, 2006), are reported for C-ALCL for the first time in this study. Telomere aggregates were observed in all three Mac cell lines and approx. 11% of all telomeric signals were aggregates. In addition to previous reports, our results are indicative of ongoing and perhaps escalating genomic instability, specifically nCIN, which may be attributable to malignant transformational processes.

I quantified telomere spatial distribution using the *a/c* ratio, which is generated for each nucleus. The distribution of the telomeres in the nuclear volume collectively can be geometrically approximated to an ellipsoid with two similar radii ($a \approx b$) and a different third one (c). The ratio of two radii that are different, a (or b) to c (*a/c* ratio), describes how flat or spherical the volume occupied by the telomeres is. Here, Mac-2B has the lowest *a/c* ratio meaning Mac-2B telomeres are organized in a more spherical 3D volume compared to the other two lines, Mac-1 3D telomeric volume is less spherical and flatter while Mac-2A telomeres are arranged in an even flatter distribution (Fig. 3E, $p < 0.05$ for all comparisons). Spatial organization of telomeres is an aspect of 3D telomere profile where data does not group the predecessor Mac-1 against later stage Mac-2A and Mac-2B; instead, Mac-1 telomere distribution

was more spherical than Mac-2B but flatter than Mac-2A. (Fig. 3E). Spatial organization of telomeres are cell cycle dependent as they can be seen to be arranging in a disc in G2 phase (Chuang et al. 2004). Since Mac-2A and Mac-2B together represent the more proliferative stage of disease, it would normally be expected that they would have a greater ratio of G2 phase cells compared to Mac-1. However, 3D telomere organization is not only dependent on cell-cycle, as the shape of the cell and therefore the shape of nucleus is also a factor which could be associated with this result. The differences of spatial telomere organization observed between these cell lines are perhaps better interpreted later, after reviewing the context of lamin A/C expression and other differences between Mac-2A and Mac-2B.

Dysregulation of lamin A/C is linked to dysregulation of DNA replication and DNA repair, both of which leads to genomic instability (Huang *et al.,* 2008, Gonzalez-Suarez *et al.,* 2009). Lamin A/C has an important role in genome organization as well, anchoring chromosomes from their telomeres by binding to a telomere associated protein and sustaining healthy telomere function (Wood *et al.,* 2014; Burla *et al.,* 2016). Therefore, cancer cells with dysregulated lamin A/C expression could either gain or lose genomic instability (based on up or down regulation of lamin A/C) both of which could confer a selective advantage to them in different tissue microenvironments. In HL, for example, lamin A/C expression is shown to be keeping genomic instability down to a sustainable level and allowing further alterations of nuclear organization in generating multinucleated large RS cells (Contu *et al.,* 2018). To describe the expression and spatial organization of lamin A/C during C-ALCL evolution, I performed immunostaining of this protein.

Here, it was observed that Mac-1 cells, which are at an earlier low level malignancy disease state (and isolated from circulating cells), already have a uniform lamin A/C expression that is not seen in the normal T lymphocytes from which they are derived (González-Granado *et al.,* 2014) (Fig 5). The later subclones, Mac-2A and Mac-2B (both isolated from skin nodules), however, appear to have altered their lamin A/C expression in different ways due to experiencing, in some form, different selection pressures (Fig 5). Mac-2A has significantly gained lamin A/C expression while Mac-2B has significantly downregulated its lamin A/C and a quarter of Mac-2B cells even appear to be lamin A/C negative (all differences have $p < 0.05$). It would be expected therefore that Mac-2B have greater genomic instability.

In a related observation, I report greater telomere lengths for Mac-2B compared to Mac-2A (Fig 3D, $p < 0.05$). It could be expected that weak lamin A/C expression of Mac-2B would lead to further telomere erosion as lamin A/C expression is necessary for telomere maintenance. However, this result is perhaps better understood as Mac-2B telomeres having longer critical lengths (compared to Mac-2A) to still be functional enough to support viable cells. In other words, Mac-2B telomeres cannot be as short as Mac-2A telomeres because they cannot function as well without lamin A/C support, potentially leading to cell death before further erosion. Still, Mac cells would be expected to have activated telomere maintenance pathways which should be normally letting them survive with short telomeres. Possible causes for differences between Mac-2A and Mac-2B are further discussed below.

Mac-2A and Mac-2B were collected on the same day, but from different ulcerating skin tumor nodules. Differences in the immunodetection of lamin A/C between these two Mac-2A/B cells lines could be indicative that Mac-2A and/or Mac-2B did not experience significant selective pressures of genome maintenance at this stage. Rather, it can be speculated that the selective pressure these subclones experienced was likely the result of advancing their metastatic potential. Lamin A/C has a positive impact on cell motility and resistance to sheer stress, but too much lamin A/C expression makes the nucleus too stiff and inhibits the cell from infiltrating tight tissue (for review of lamin A/C and cell motility, Dubik & Mai, 2020). It has been established in various cancers that downregulation or upregulation of lamin A/C has an effect on cancer cell infiltration of neighboring tissues (Dubik & Mai, 2020). Derived from originally circulating cancer cells that have infiltrated into skin tissue, heterogeneous lamin A/C expressing Mac-2A and Mac-2B cells could have undergone a selection stemming from the unique difficulties of invading the skin nodules from which they were biopsied. In future studies, the role of lamin A/C in C-ALCL cell motility in comparison to genome maintenance may be tested by inhibiting lamin A/C in these cell lines and observing the outcome on motility and survival. Here, I can conclude that Mac-1 representing an early less aggressive C-ALCL stage appears to have sufficient control of its genome organization to the extent that Mac-1 can afford to lose most of its lamin A/C expression when evolving to Mac-2B.

I have observed multinucleated cells, which are much more prominent in the later Mac-2A and Mac-2B to a ratio of about 10% of the population (Fig 6.). Multinucleated cells of Mac

lines can be of lymphocyte size, like the most of their population, or of larger size. The large, atypical subpopulation was reported as resembling multinucleated RS cells of HL (Davis *et al.,* 1992). In this thesis, large-cells, both mononucleated and multinucleated, again make about 10% of the Mac-2A and Mac-2B populations. In HL, mononucleated H cells transition into multinucleated RS cells by accumulating further genome remodeling such as changing their 3D telomere profile (Knecht *et al.,* 2009). An overexpression of lamin A/C, abnormally localized to interior of nucleus, is associated and necessary for this transition (Contu *et al.,* 2018). I wanted to see if there were signs that a similar change of 3D telomere profile could be associated with the generation of multinucleated C-ALCL cells from mononucleated cells and if lamin A/C could be playing a similar role. So, I again looked at telomere Q-FISH and lamin A/C immunostaining data by analyzing mononucleated cells against the multinucleated.

Before discussing quantified data, I report that lamin A/C structure was found uniformly at the nuclear periphery across all Mac lines, mostly appearing as a complete or sometimes partial ring in both mononuclear and multinuclear cells, similar to its appearance in activated lymphocytes (Fig 4). This contrasts with HL, where mononucleated H cells can be categorized based on how extensively internal lamin A/C structures compartmentalize the nucleus (Contu *et al.,* 2018). Mac-2A multinucleated cells did not show a difference of lamin A/C expression compared to mononucleated Mac-2A cells. Mac-2B multinucleated cells, however, did show significantly greater lamin A/C expression (Fig 8. $p < 0.05$) compared to mononucleated Mac-2B cells. It is plausible to interpret this difference in context with Mac-2B cells having normally very little to no lamin A/C expression, especially compared to Mac-2A. It could be that Mac-2B cells are at a critical stage and further genome remodeling to multinucleation at this stage is unsustainable for them, without once again selecting for upregulating lamin A/C expression. This change in Mac-2B lamin A/C expression associated with multinucleation is the only parallel that could be drawn with the multinucleation process of HL. Whether lamin A/C is necessary for the multinucleation process of C-ALCL can only be established by future studies that inhibit lamin A/C to observe whether multinucleated cells are sustained in culture.

This study found that multinucleation in C-ALCL can be associated with remodeling of 3D telomere profile. Multinucleated cells had more telomeres compared to mononucleated cells ($p < 0.05$) indicating that DNA replication is functional before cytokinetic failure, leading to

chromosomal gains. Telomere aggregates were observed in multinucleated cells but their ratio to normal telomeric signals was unchanged, indicating no acceleration of BFB cycles (Mai & Garini, 2006). Multinucleated Mac-2A cells had longer telomeres compared to mononucleated Mac-2A cells (Fig 7A, $p < 0.05$) while multinucleated Mac-2B cells had shorter telomeres compared to mononucleated Mac-2B cells (Fig 7B, $p < 0.05$). Once again it is not possible to directly attribute these differences between Mac-2A and Mac-2B to their lamin A/C expressions; experiments that inhibit lamin A/C may reveal a link. Theoretically, however, it makes sense that the cell line with lesser lamin A/C expression (Mac-2B) would not be able to maintain its telomeres as well through multinucleation, considering the role of lamin A/C in telomere maintenance (Wood *et al.,* 2014; Burla *et al.,* 2016) and its necessity for viable telomere organization of multinucleated cells in other diseases such as HL (Contu *et al.,* 2018). Both Mac-2A and Mac-2B multinucleation processes were associated with a spatial reorganization of telomeres into a flatter 3D volume, indicative of G2 phase (Fig 7C-D, $p < 0.05$, Chuang et al. 2004). This could be due to stalling cytokinesis, a phenotype that has been associated with multinucleation process in other lymphomas (Rengstl et al., 2013) or increased proliferation.

I also analyzed a trio of malignant C-ALCL tissue samples in order to initiate an exploration of their heterogeneity in terms of genome organization, specifically of 3D telomere profiles and lamina structures. JS10 was a sample collected from lymph node biopsy, LS21 was biopsied from near a breast implant and is a special case of C-ALCL called breast implant associated-ALCL (BIA-ALCL), while Margie89 was a tissue sample collected from a skin lesion like Mac-2A and Mac-2B (Table 1 for references).

With regards to telomere profiles, LS21 telomeres are observed here to be fewer in number compared to the other lines, indicating a further loss of chromosomes on average in that line (Fig 9C, $p < 0.05$). This alone is not indicative of a heterogeneity in genome organization or instability by itself (Lengauer *et al.,* 1998). Other significant differences were observed, however the data from that section of this study is too limited to discuss at this stage.

Summary, Conclusions and Future directions

Summary

In this study, I have characterized alterations of genome organization C-ALCL cells can have through a low to high malignancy disease transformation using the Mac cell lines. An erosion of telomere lengths as well as a gain of chromosomes were quantifiable changes that are associated with this cancer evolution. Chromosomal gains in this study were quantified here for the first time from samples of a single clonal background at consecutive timepoints. Therefore, they are indicative of ongoing genomic instability, a phenotype that likely is a driving force of C-ALCL transformation.

3D telomere profile differences were not the only differences observed between early and late-stage C-ALCL. Significant telomere length and telomere spatial distribution differences between subclones of same late-stage C-ALCL are reported in this study as well.

I also documented C-ALCL cells to be lamin A/C expressing at an early stage of disease and capable of later downregulating or upregulating this expression during a malignant transformation. Unlike HL (Contu *et al.*, 2018), I observed that dysregulated lamin A/C is not localized to nuclear interior in C-ALCL.

Finally, some of the genome remodelling C-ALCL cells undergo through the multinucleation process in late disease stage are characterized in this study. I observed that an advanced stage C-ALCL cell line with weak lamin A/C expression produced multinucleated cells that increased their lamin A/C expression and had further telomere erosion. Meanwhile another advanced stage C-ALCL cell line with strong lamin A/C expression produced multinucleated cells that had longer telomeres.

Conclusions

Previous groups have profiled the genome of multiple C-ALCL cases and cell lines which has generated data on general frequency of chromosomal abnormalities and single

nucleotide polymorphisms in C-ALCL (for review of ALCL genetics, Zeng & Feldman, 2015). However, genome alteration, through a malignant transformation or genome alterations over time in general, had not been investigated until this study. Genomic instability of C-ALCL is therefore also currently not well understood. Despite the amount of data on copy number abnormalities of ALCL, the clinical relevance of these findings is so far unestablished. Therefore, copy number testing or other genome profiling is not performed routinely for C-ALCL in the clinic.

The results from Mac cell lines in this study represent one case of C-ALCL, they are therefore not sufficient to establish general trends of C-ALCL disease. My results in this study serve as a preliminary analysis of one possible path genome alterations can develop during the progress of C-ALCL disease. We now have first insights on the extent and heterogeneity of genome organization alterations this disease can obtain over time, as well as levels of genomic instability associated with it.

It can be concluded from these results that an ongoing genome instability and resulting net chromosomal gain can be associated with malignant transformation in C-ALCL, as observed here by an increase in telomeric signals when comparing early-stage Mac-1 and late-stage Mac-2A, Mac-2B. It is possible that in other C-ALCL cases, or in general in C-ALCL, a net loss of chromosomes is instead a driver of malignant transformation. For other CTCL, like mycosis fungoides (MF) and Sezary Syndrome (SS), %35 fewer telomere signals on average were detected in diseased cells compared to control lymphocytes, indicating a general trend of chromosomal losses with cancer progression. (Bienz *et al.*, 2021).

Another conclusion we reach is that C-ALCL can have subclones with significantly heterogenous nuclear organization at late stages, as evidenced by multiple differences between Mac-2A and Mac-2B such as flexible lamin A/C phenotypes with currently unknown selective advantages for the subpopulations. It is again possible that other advanced C-ALCL cases have more homogenous lamina organization. The increase in heterogeneity of nuclear organization throughout C-ALCL progression is also evident from the emergence of subpopulations of mono- and multinucleated cells.

With regards to the multinucleation process of C-ALCL: Although there are signs that at least some lamin A/C expression could be required for viable multinucleated cells, it can be

concluded here that the nuclear remodelling required for transformation to “RS-like” cells in this disease does not necessarily follow the nuclear remodelling H cells undergo during their transformation to RS cells in HL. There are changes to 3D telomere profile during the multinucleation process, however it is too early at this point to draw a conclusion about the significance of these changes to the disease progress.

The extension of experiments in this study to tissue samples was meant to serve as a baseline for future studies, showing what data can be generated using telomere FISH and co-immunostaining with tissue samples of different sources. I have observed some significant differences of nuclear organization between tissue samples; however, it is too early to attribute these differences to the pathophysiology of these unique samples.

Future Directions

There are multiple directions future studies could advance to build up on this preliminary study. The most crucial would be to simply expand the framework of this study by comparing more early and advanced disease stages of C-ALCL, ideally from the same patient, with a further focus on tissue samples. This would allow a better understanding of disease-wide heterogeneity and general trends of nuclear organization changes that govern malignant transformation of C-ALCL. Such data could potentially then be used in predictive models of disease progression with clinically relevant prognostic value, that could guide treatment choices and advance our ability to combat C-ALCL. Perhaps more importantly, such an advancement in our understanding of C-ALCL pathophysiology would also give us a clearer view of why C-ALCL remains one of the most treatable hematological malignancies and enable us to isolate key differences of other hematological malignancies that make them more dangerous.

While the data from the tissue samples in this study were not deemed sufficient to reach significant conclusions, they may contribute to a future study aimed at identifying key differences of diseased nuclear organization of samples derived from different tissue microenvironments in C-ALCL.

To clearly understand the pathophysiology of multinucleated late-stage cells, monitoring of the multinucleation phenotype upon specifically targeted RNA interference of lamin A/C knockdown may establish new roles of lamin A/C for the process. Similar experiments could be

designed to target telomere associated proteins, such as telomerase, to understand the significance of 3D telomere profile changes associated with multinucleation in in C-ALCL.

Limitations

Cell line cultures, which were used in this study, have known limitations as cancer models. Extended cultures can alter the genome organization (Domcke et al., 2013) and expression patterns (Chen et al., 2015) of unstable cell lines to the point where they have limited potential in representing their primary tumor. In this study, cells were used for experiments after a single passage. Results here are also in line with previous research. Telomere counts, for example, are observed to be similar between advanced Mac-2A-Mac-2B and fewer in early Mac-1 which aligns with previous observations of chromosome counts (Davis *et al.,* 1992).

As stated above, this study mostly examines a single case of C-ALCL and experimentally initiates a wider tissue study. The conclusions reached are informative of a possible path: genome alterations can develop in C-ALCL and are not meant to represent the general trends of this disease until further studies.

References

1. Hertwig, O. (1876). Beiträge zur Kenntnis der Bildung, Befruchtung und Theilung des thierischen Eies. *Morphologisches Jahrbuch*, 347–434.
2. Hertwig, O. (1877). Beiträge zur Kenntnis der Bildung, Befruchtung und Theilung des thierischen Eies II. *Morphologisches Jahrbuch*, 1-86.
3. Hertwig, O. (1878). Beiträge zur Kenntnis der Bildung, Befruchtung und Theilung des thierischen Eies III. *Morphologisches Jahrbuch*, 156-213.
4. van Beneden E. (1883) Recherches sur la Maturation de L´Oeuf, la Fécondation et la Division Cellulaire
5. Rabl C. Über Zelltheilung. (1885) *Morphologisches Jahrbuch* 10:214-330.
6. Cremer, T., & Cremer, C. (2006). Rise, fall and resurrection of chromosome territories: a historical perspective. Part I. The rise of chromosome territories. European journal of histochemistry : EJH, 50(3), 161–176.
7. Monneron, A., & Bernhard, W. (1969). Fine structural organization of the interphase nucleus in some mammalian cells. *Journal of Ultrastructure Research*, *27*(3–4), 266–288. https://doi.org/10.1016/s0022-5320(69)80017-1
8. Boveri T. (1888) Zellen Studien II. Die Befruchtung und Teilung des Eies von Ascaris megalocephala. 685-882.
9. Boveri T. (1909) Die Blastomerenkerne von Ascaris megalocephala und die Theorie der Chromosomenindividualität. Arch Zellforsch 3:181-268
10. Cremer, T., Cremer, C., & Lichter, P. (2014). Recollections of a scientific journey published in human genetics: from chromosome territories to interphase cytogenetics and comparative genome hybridization. Human Genetics, 133(4), 403–416. https://doi.org/10.1007/s00439-014-1425-5
11. Cremer, T., Cremer, M., Hübner, B., Strickfaden, H., Smeets, D., Popken, J., Sterr, M., Markaki, Y., Rippe, K., & Cremer, C. (2015). The 4D nucleome: Evidence for a dynamic nuclear landscape based on co-aligned active and inactive nuclear compartments. FEBS Letters, 589(20PartA), 2931–2943. https://doi.org/10.1016/j.febslet.2015.05.037

12. Maeshima, K., Ide, S., & Babokhov, M. (2019). Dynamic chromatin organization without the 30-nm fiber. Current Opinion in Cell Biology, 58, 95–104. https://doi.org/10.1016/j.ceb.2019.02.003
13. Vermunt, M. W., Zhang, D., & Blobel, G. A. (2018). The interdependence of gene-regulatory elements and the 3D genome. Journal of Cell Biology, 218(1), 12–26. https://doi.org/10.1083/jcb.201809040
14. Dekker, J., & Misteli, T. (2015). Long-Range Chromatin Interactions. Cold Spring Harbor Perspectives in Biology, 7(10), a019356. https://doi.org/10.1101/cshperspect.a019356
15. Dekker, J., Rippe, K., Dekker, M., & Kleckner, N. (2002). Capturing Chromosome Conformation. Science, 295(5558), 1306–1311. https://doi.org/10.1126/science.1067799
16. Misteli, T. (2020). The Self-Organizing Genome: Principles of Genome Architecture and Function. Cell, 183(1), 28–45. https://doi.org/10.1016/j.cell.2020.09.014
17. Fudenberg, G., Imakaev, M., Lu, C., Goloborodko, A., Abdennur, N., & Mirny, L. (2016). Formation of Chromosomal Domains by Loop Extrusion. Cell Reports, 15(9), 2038–2049. https://doi.org/10.1016/j.celrep.2016.04.085
18. Shopland, L. S., Lynch, C. R., Peterson, K. A., Thornton, K., Kepper, N., Hase, J. V., Stein, S., Vincent, S., Molloy, K. R., Kreth, G., Cremer, C., Bult, C. J., & O'Brien, T. P. (2006). Folding and organization of a contiguous chromosome region according to the gene distribution pattern in primary genomic sequence. Journal of Cell Biology, 174(1), 27–38. https://doi.org/10.1083/jcb.200603083
19. Beagrie, R. A., Scialdone, A., Schueler, M., Kraemer, D. C. A., Chotalia, M., Xie, S. Q., Barbieri, M., de Santiago, I., Lavitas, L. M., Branco, M. R., Fraser, J., Dostie, J., Game, L., Dillon, N., Edwards, P. A. W., Nicodemi, M., & Pombo, A. (2017). Complex multi-enhancer contacts captured by genome architecture mapping. Nature, 543(7646), 519–524. https://doi.org/10.1038/nature21411
20. Wang, S., Su, J. H., Beliveau, B. J., Bintu, B., Moffitt, J. R., Wu, C. T., & Zhuang, X. (2017). Spatial Organization of Chromatin Domains and Compartments in Single Chromosomes. Biophysical Journal, 112(3), 217a. https://doi.org/10.1016/j.bpj.2016.11.1199

21. Fraser, J., Ferrai, C., Chiariello, A. M., Schueler, M., Rito, T., Laudanno, G., Barbieri, M., Moore, B. L., Kraemer, D. C., Aitken, S., Xie, S. Q., Morris, K. J., Itoh, M., Kawaji, H., Jaeger, I., Hayashizaki, Y., Carninci, P., Forrest, A. R., Semple, C. A., . . . Nicodemi, M. (2015). Hierarchical folding and reorganization of chromosomes are linked to transcriptional changes in cellular differentiation. Molecular Systems Biology, 11(12), 852. https://doi.org/10.15252/msb.20156492
22. Cremer, T., & Cremer, M. (2010). Chromosome Territories. Cold Spring Harbor Perspectives in Biology, 2(3), a003889. https://doi.org/10.1101/cshperspect.a003889
23. Zorn, C., Cremer, C., Cremer, T., & Zimmer, J. (1979). Unscheduled DNA synthesis after partial UV irradiation of the cell nucleus. Experimental Cell Research, 124(1), 111–119. https://doi.org/10.1016/0014-4827(79)90261-1
24. Lichter, P., Cremer, T., Borden, J., Manuelidis, L., & Ward, D. C. (1988). Delineation of individual human chromosomes in metaphase and interphase cells by in situ suppression hybridization using recombinant DNA libraries. Human Genetics, 80(3), 224–234. https://doi.org/10.1007/bf01790090
25. Fawcett, D. W. (1966). On the occurrence of a fibrous lamina on the inner aspect of the nuclear envelope in certain cells of vertebrates. American Journal of Anatomy, 119(1), 129–145. https://doi.org/10.1002/aja.1001190108
26. Ferreira, J., Paolella, G., Ramos, C., & Lamond, A. I. (1997). Spatial Organization of Large-Scale Chromatin Domains in the Nucleus: A Magnified View of Single Chromosome Territories. Journal of Cell Biology, 139(7), 1597–1610. https://doi.org/10.1083/jcb.139.7.1597
27. Lieberman-Aiden, E., van Berkum, N. L., Williams, L., Imakaev, M., Ragoczy, T., Telling, A., Amit, I., Lajoie, B. R., Sabo, P. J., Dorschner, M. O., Sandstrom, R., Bernstein, B., Bender, M. A., Groudine, M., Gnirke, A., Stamatoyannopoulos, J., Mirny, L. A., Lander, E. S., & Dekker, J. (2009). Comprehensive Mapping of Long-Range Interactions Reveals Folding Principles of the Human Genome. Science, 326(5950), 289–293. https://doi.org/10.1126/science.1181369

28. Rowley, M. J., & Corces, V. G. (2018). Organizational principles of 3D genome architecture. Nature Reviews Genetics, 19(12), 789–800. https://doi.org/10.1038/s41576-018-0060-8
29. Sadoni, N., Langer, S., Fauth, C., Bernardi, G., Cremer, T., Turner, B. M., & Zink, D. (1999). Nuclear Organization of Mammalian Genomes. *Journal of Cell Biology*, *146*(6), 1211–1226. https://doi.org/10.1083/jcb.146.6.1211
30. Shevelyov, Y. Y., & Ulianov, S. V. (2019). The Nuclear Lamina as an Organizer of Chromosome Architecture. Cells, 8(2), 136. https://doi.org/10.3390/cells8020136
31. Solovei, I., Wang, A., Thanisch, K., Schmidt, C., Krebs, S., Zwerger, M., Cohen, T., Devys, D., Foisner, R., Peichl, L., Herrmann, H., Blum, H., Engelkamp, D., Stewart, C., Leonhardt, H., & Joffe, B. (2013). LBR and Lamin A/C Sequentially Tether Peripheral Heterochromatin and Inversely Regulate Differentiation. *Cell*, *152*(3), 584–598. https://doi.org/10.1016/j.cell.2013.01.009
32. Zheng, X., Hu, J., Yue, S., Kristiani, L., Kim, M., Sauria, M., Taylor, J., Kim, Y., & Zheng, Y. (2018). Lamins Organize the Global Three-Dimensional Genome from the Nuclear Periphery. Molecular Cell, 71(5), 802–815.e7. https://doi.org/10.1016/j.molcel.2018.05.017
33. Kumaran, R. I., & Spector, D. L. (2008). A genetic locus targeted to the nuclear periphery in living cells maintains its transcriptional competence. Journal of Cell Biology, 180(1), 51–65. https://doi.org/10.1083/jcb.200706060
34. Finlan, L. E., Sproul, D., Thomson, I., Boyle, S., Kerr, E., Perry, P., Ylstra, B., Chubb, J. R., & Bickmore, W. A. (2008). Recruitment to the Nuclear Periphery Can Alter Expression of Genes in Human Cells. PLoS Genetics, 4(3), e1000039. https://doi.org/10.1371/journal.pgen.1000039
35. Reddy, K. L., Zullo, J. M., Bertolino, E., & Singh, H. (2008). Transcriptional repression mediated by repositioning of genes to the nuclear lamina. Nature, 452(7184), 243–247. https://doi.org/10.1038/nature06727
36. Wang, H., Xu, X., Nguyen, C. M., Liu, Y., Gao, Y., Lin, X., Daley, T., Kipniss, N. H., La Russa, M., & Qi, L. S. (2018). CRISPR-Mediated Programmable 3D Genome Positioning

and Nuclear Organization. Cell, 175(5), 1405–1417.e14. https://doi.org/10.1016/j.cell.2018.09.013

37. Boyle, S. (2001). The spatial organization of human chromosomes within the nuclei of normal and emerin-mutant cells. Human Molecular Genetics, 10(3), 211–219. https://doi.org/10.1093/hmg/10.3.211
38. Tanabe, H., Müller, S., Neusser, M., von Hase, J., Calcagno, E., Cremer, M., Solovei, I., Cremer, C., & Cremer, T. (2002). Evolutionary conservation of chromosome territory arrangements in cell nuclei from higher primates. Proceedings of the National Academy of Sciences, 99(7), 4424–4429. https://doi.org/10.1073/pnas.072618599
39. Bolzer, A., Kreth, G., Solovei, I., Koehler, D., Saracoglu, K., Fauth, C., Müller, S., Eils, R., Cremer, C., Speicher, M. R., & Cremer, T. (2005). Three-Dimensional Maps of All Chromosomes in Human Male Fibroblast Nuclei and Prometaphase Rosettes. PLoS Biology, 3(5), e157. https://doi.org/10.1371/journal.pbio.0030157
40. Griffith, J. D., Comeau, L., Rosenfield, S., Stansel, R. M., Bianchi, A., Moss, H., & de Lange, T. (1999). Mammalian Telomeres End in a Large Duplex Loop. *Cell*, *97*(4), 503–514. https://doi.org/10.1016/s0092-8674(00)80760-6
41. Scherthan, H., Jerratsch, M., Li, B., Smith, S., Hultén, M., Lock, T., & de Lange, T. (2000). Mammalian Meiotic Telomeres: Protein Composition and Redistribution in Relation to Nuclear Pores. Molecular Biology of the Cell, 11(12), 4189–4203. https://doi.org/10.1091/mbc.11.12.4189
42. Crabbe, L., Cesare, A., Kasuboski, J., Fitzpatrick, J., & Karlseder, J. (2012). Human Telomeres Are Tethered to the Nuclear Envelope during Postmitotic Nuclear Assembly. Cell Reports, 2(6), 1521–1529. https://doi.org/10.1016/j.celrep.2012.11.019
43. Bronshtein, I., Kepten, E., Kanter, I., Berezin, S., Lindner, M., Redwood, A. B., Mai, S., Gonzalo, S., Foisner, R., Shav-Tal, Y., & Garini, Y. (2015). Loss of lamin A function increases chromatin dynamics in the nuclear interior. Nature Communications, 6(1). https://doi.org/10.1038/ncomms9044
44. Burla, R., La Torre, M., & Saggio, I. (2016). Mammalian telomeres and their partnership with lamins. Nucleus, 7(2), 187–202. https://doi.org/10.1080/19491034.2016.1179409

45. Gonzalez-Suarez, I., Redwood, A. B., & Gonzalo, S. (2009). Loss of A-type lamins and genomic instability. Cell Cycle, 8(23), 3860–3865. https://doi.org/10.4161/cc.8.23.10092
46. Gonzalez-Suarez, I., Redwood, A. B., Perkins, S. M., Vermolen, B., Lichtensztejin, D., Grotsky, D. A., Morgado-Palacin, L., Gapud, E. J., Sleckman, B. P., Sullivan, T., Sage, J., Stewart, C. L., Mai, S., & Gonzalo, S. (2009). Novel roles for A-type lamins in telomere biology and the DNA damage response pathway. The EMBO Journal, 28(16), 2414–2427. https://doi.org/10.1038/emboj.2009.196
47. Chuang, T. C., Moshir, S., Garini, Y., Chuang, A. Y., Young, I. T., Vermolen, B., van den Doel, R., Mougey, V., Perrin, M., Braun, M., Kerr, P. D., Fest, T., Boukamp, P., & Mai, S. (2004). The three-dimensional organization of telomeres in the nucleus of mammalian cells. *BMC biology*, *2*, 12. https://doi.org/10.1186/1741-7007-2-12
48. Kempfer, R., & Pombo, A. (2019). Methods for mapping 3D chromosome architecture. Nature Reviews Genetics, 21(4), 207–226. https://doi.org/10.1038/s41576-019-0195-2
49. Kong, S., & Zhang, Y. (2019). Deciphering Hi-C: from 3D genome to function. *Cell Biology and Toxicology*, *35*(1), 15–32. https://doi.org/10.1007/s10565-018-09456-2
50. Simonis, M., Kooren, J., & de Laat, W. (2007). An evaluation of 3C-based methods to capture DNA interactions. *Nature Methods*, *4*(11), 895–901. https://doi.org/10.1038/nmeth1114
51. Nagano, T., Lubling, Y., Várnai, C., Dudley, C., Leung, W., Baran, Y., Mendelson Cohen, N., Wingett, S., Fraser, P., & Tanay, A. (2017). Cell-cycle dynamics of chromosomal organization at single-cell resolution. Nature, 547(7661), 61–67. https://doi.org/10.1038/nature23001
52. Spilianakis, C. G., Lalioti, M. D., Town, T., Lee, G. R., & Flavell, R. A. (2005). Interchromosomal associations between alternatively expressed loci. Nature, 435(7042), 637–645. https://doi.org/10.1038/nature03574
53. Nagano, T., Lubling, Y., Yaffe, E., Wingett, S. W., Dean, W., Tanay, A., & Fraser, P. (2015). Single-cell Hi-C for genome-wide detection of chromatin interactions that occur simultaneously in a single cell. Nature Protocols, 10(12), 1986–2003. https://doi.org/10.1038/nprot.2015.127

54. Rao, S., Huntley, M., Durand, N., Stamenova, E., Bochkov, I., Robinson, J., Sanborn, A., Machol, I., Omer, A., Lander, E., & Aiden, E. (2015). A 3D Map of the Human Genome at Kilobase Resolution Reveals Principles of Chromatin Looping. Cell, 162(3), 687–688. https://doi.org/10.1016/j.cell.2015.07.024
55. Speicher, M. R., Ballard, S. G., & Ward, D. C. (1996). Karyotyping human chromosomes by combinatorial multi-fluor FISH. Nature Genetics, 12(4), 368–375. https://doi.org/10.1038/ng0496-368
56. Takei, Y., Shah, S., Harvey, S., Qi, L. S., & Cai, L. (2017). Multiplexed Dynamic Imaging of Genomic Loci by Combined CRISPR Imaging and DNA Sequential FISH. *Biophysical Journal*, *112*(9), 1773–1776. https://doi.org/10.1016/j.bpj.2017.03.024
57. Lubeck, E., Coskun, A. F., Zhiyentayev, T., Ahmad, M., & Cai, L. (2014). Single-cell in situ RNA profiling by sequential hybridization. *Nature Methods*, *11*(4), 360–361. https://doi.org/10.1038/nmeth.2892
58. Shah, S., Lubeck, E., Zhou, W., & Cai, L. (2016). In Situ Transcription Profiling of Single Cells Reveals Spatial Organization of Cells in the Mouse Hippocampus. *Neuron*, *92*(2), 342–357. https://doi.org/10.1016/j.neuron.2016.10.001
59. Takei, Y., Yun, J., Zheng, S., Ollikainen, N., Pierson, N., White, J., Shah, S., Thomassie, J., Suo, S., Eng, C. H. L., Guttman, M., Yuan, G. C., & Cai, L. (2021). Integrated spatial genomics reveals global architecture of single nuclei. *Nature*, *590*(7845), 344–350. https://doi.org/10.1038/s41586-020-03126-2
60. Ma, H., Tu, L. C., Naseri, A., Huisman, M., Zhang, S., Grunwald, D., & Pederson, T. (2016). Multiplexed labeling of genomic loci with dCas9 and engineered sgRNAs using CRISPRainbow. Nature Biotechnology, 34(5), 528–530. https://doi.org/10.1038/nbt.3526
61. Boettiger, A. N., Bintu, B., Moffitt, J. R., Wang, S., Beliveau, B. J., Fudenberg, G., Imakaev, M., Mirny, L. A., Wu, C. T., & Zhuang, X. (2016). Super-resolution imaging reveals distinct chromatin folding for different epigenetic states. Nature, 529(7586), 418–422. https://doi.org/10.1038/nature16496
62. Young, I. T., Verbeek, P. W., & Mayall, B. H. (1986). Characterization of chromatin distribution in cell nuclei. Cytometry, 7(5), 467–474. https://doi.org/10.1002/cyto.990070513

63. Righolt, C. H., Guffei, A., Knecht, H., Young, I. T., Stallinga, S., van Vliet, L. J., & Mai, S. (2014). Differences in Nuclear DNA Organization Between Lymphocytes, Hodgkin and Reed–Sternberg Cells Revealed by Structured Illumination Microscopy. Journal of Cellular Biochemistry, 115(8), 1441–1448. https://doi.org/10.1002/jcb.24800
64. Schmälter AK, Kuzyk A, Righolt CH, et al. Distinct nuclear orientation patterns for mouse chromosome 11 in normal B lymphocytes. BMC Cell Biol. 2014;15:22.
65. Schmälter AK, Righolt CH, Kuzyk A, Mai S. Changes in nuclear orientation patterns of chromosome 11 during mouse plasmacytoma development. Transl Oncol. 2015; 8(5):417-23
66. Krijger, P. H. L., & de Laat, W. (2016). Regulation of disease-associated gene expression in the 3D genome. Nature Reviews Molecular Cell Biology, 17(12), 771–782. https://doi.org/10.1038/nrm.2016.138
67. Spielmann, M., Lupiáñez, D. G., & Mundlos, S. (2018). Structural variation in the 3D genome. Nature Reviews Genetics, 19(7), 453–467. https://doi.org/10.1038/s41576-018-0007-0
68. Dekker, J., Belmont, A. S., Guttman, M., Leshyk, V. O., Lis, J. T., Lomvardas, S., Mirny, L. A., O'Shea, C. C., Park, P. J., Ren, B., Politz, J. C. R., Shendure, J., & Zhong, S. (2017). The 4D nucleome project. Nature, 549(7671), 219–226. https://doi.org/10.1038/nature23884
69. Keightley, P. D. (2012). Rates and Fitness Consequences of New Mutations in Humans. Genetics, 190(2), 295–304. https://doi.org/10.1534/genetics.111.134668
70. Von Hansemann, D. (1890) Ueber asymmetrische Zellteilung in Epithelkrebsen und deren biologische Bedeutung. Virchows Arch. Patholog. Anat. 119, 299–326
71. Boveri, T. (1914) Zur frage der enstehung maligner tumoren (Gustav Fischer Verlag, Jena, (in German)
72. Nowell, P. C. (1976). The Clonal Evolution of Tumor Cell Populations. Science, 194(4260), 23–28. https://doi.org/10.1126/science.959840
73. Lengauer, C., Kinzler, K. W., & Vogelstein, B. (1997). Genetic instability in colorectal cancers. Nature, 386(6625), 623–627. https://doi.org/10.1038/386623a0

74. Antonarakis, S. E., Lyle, R., Dermitzakis, E. T., Reymond, A., & Deutsch, S. (2004). Chromosome 21 and Down syndrome: from genomics to pathophysiology. *Nature Reviews Genetics*, *5*(10), 725–738. https://doi.org/10.1038/nrg1448
75. Bayani, J., Selvarajah, S., Maire, G., Vukovic, B., Al-Romaih, K., Zielenska, M., & Squire, J. A. (2007). Genomic mechanisms and measurement of structural and numerical instability in cancer cells. *Seminars in Cancer Biology*, *17*(1), 5–18. https://doi.org/10.1016/j.semcancer.2006.10.006
76. Negrini, S., Gorgoulis, V. G., & Halazonetis, T. D. (2010). Genomic instability — an evolving hallmark of cancer. Nature Reviews Molecular Cell Biology, 11(3), 220–228. https://doi.org/10.1038/nrm2858
77. Hanahan, D., & Weinberg, R. (2011). Hallmarks of Cancer: The Next Generation. Cell, 144(5), 646–674. https://doi.org/10.1016/j.cell.2011.02.013
78. Li, K., Luo, H., Huang, L., Luo, H., & Zhu, X. (2020). Microsatellite instability: a review of what the oncologist should know. Cancer Cell International, 20(1). https://doi.org/10.1186/s12935-019-1091-8
79. Olivier, M., Hollstein, M., & Hainaut, P. (2009). TP53 Mutations in Human Cancers: Origins, Consequences, and Clinical Use. Cold Spring Harbor Perspectives in Biology, 2(1), a001008. https://doi.org/10.1101/cshperspect.a001008 https://doi.org/10.1126/science.1133427
80. Kennedy, R. D., & D'Andrea, A. D. (2006). DNA Repair Pathways in Clinical Practice: Lessons From Pediatric Cancer Susceptibility Syndromes. Journal of Clinical Oncology, 24(23), 3799–3808. https://doi.org/10.1200/jco.2005.05.4171
81. Ripperger, T., Gadzicki, D., Meindl, A., & Schlegelberger, B. (2008). Breast cancer susceptibility: current knowledge and implications for genetic counselling. European Journal of Human Genetics, 17(6), 722–731. https://doi.org/10.1038/ejhg.2008.212
82. Bachrati, c. z., & Hickson. (2003). RecQ helicases: suppressors of tumorigenesis and premature aging. Biochemical Journal, 374(3), 577–606. https://doi.org/10.1042/bj20030491
83. Shay, J. W., & Wright, W. E. (2000). Hayflick, his limit, and cellular ageing. Nature Reviews Molecular Cell Biology, 1(1), 72–76. https://doi.org/10.1038/35036093

84. van Steensel, B., Smogorzewska, A., & de Lange, T. (1998). TRF2 Protects Human Telomeres from End-to-End Fusions. Cell, 92(3), 401–413. https://doi.org/10.1016/s0092-8674(00)80932-0
85. Liddiard, K., Ruis, B., Takasugi, T., Harvey, A., Ashelford, K. E., Hendrickson, E. A., & Baird, D. M. (2016). Sister chromatid telomere fusions, but not NHEJ-mediated inter-chromosomal telomere fusions, occur independently of DNA ligases 3 and 4. Genome Research, 26(5), 588–600. https://doi.org/10.1101/gr.200840.115
86. Rai, R., Zheng, H., He, H., Luo, Y., Multani, A., Carpenter, P. B., & Chang, S. (2010). The function of classical and alternative non-homologous end-joining pathways in the fusion of dysfunctional telomeres. The EMBO Journal, 29(15), 2598–2610. https://doi.org/10.1038/emboj.2010.142
87. Cleal, K., Norris, K., & Baird, D. (2018). Telomere Length Dynamics and the Evolution of Cancer Genome Architecture. International Journal of Molecular Sciences, 19(2), 482. https://doi.org/10.3390/ijms19020482
88. Kolquist, K. A., Ellisen, L. W., Counter, C. M., Meyerson, M. M., Tan, L. K., Weinberg, R. A., Haber, D. A., & Gerald, W. L. (1998). Expression of TERT in early premalignant lesions and a subset of cells in normal tissues. Nature Genetics, 19(2), 182–186. https://doi.org/10.1038/554
89. Mai, S. (2010). Initiation of telomere-mediated chromosomal rearrangements in cancer. *Journal of Cellular Biochemistry*, n/a. https://doi.org/10.1002/jcb.22501
90. Lengauer, C., Kinzler, K. W., & Vogelstein, B. (1998). Genetic instabilities in human cancers. Nature, 396(6712), 643–649. https://doi.org/10.1038/25292
91. Bunz, F. et al. (2002) Targeted inactivation of p53 in human cells does not result in aneuploidy. Cancer Res. 62, 1129–1133
92. Geigl, J. B., Obenauf, A. C., Schwarzbraun, T., & Speicher, M. R. (2008). Defining 'chromosomal instability.' *Trends in Genetics*, *24*(2), 64–69. https://doi.org/10.1016/j.tig.2007.11.006
93. Pikor, L., Thu, K., Vucic, E., & Lam, W. (2013). The detection and implication of genome instability in cancer. *Cancer and Metastasis Reviews*, *32*(3–4), 341–352. https://doi.org/10.1007/s10555-013-9429-5

94. Bayani, J., & Squire, J. (2001). Advances in the detection of chromosomal aberrations using spectral karyotyping. *Clinical Genetics*, *59*(2), 65–73. https://doi.org/10.1034/j.1399-0004.2001.590201.x
95. Louis, S. F., Vermolen, B. J., Garini, Y., Young, I. T., Guffei, A., Lichtensztejn, Z., Kuttler, F., Chuang, T. C. Y., Moshir, S., Mougey, V., Chuang, A. Y. C., Kerr, P. D., Fest, T., Boukamp, P., & Mai, S. (2005). c-Myc induces chromosomal rearrangements through telomere and chromosome remodeling in the interphase nucleus. *Proceedings of the National Academy of Sciences*, *102*(27), 9613–9618. https://doi.org/10.1073/pnas.0407512102
96. Vermolen, B. J., Garini, Y., Mai, S., Mougey, V., Fest, T., Chuang, T. C. Y., Chuang, A. Y. C., Wark, L., & Young, I. T. (2005). Characterizing the three-dimensional organization of telomeres. *Cytometry Part A*, *67A*(2), 144–150. https://doi.org/10.1002/cyto.a.20159
97. Sathitruangsak, C., Righolt, C. H., Klewes, L., Tung Chang, D., Kotb, R., & Mai, S. (2016). Distinct and shared three-dimensional chromosome organization patterns in lymphocytes, monoclonal gammopathy of undetermined significance and multiple myeloma. International Journal of Cancer, 140(2), 400–410. https://doi.org/10.1002/ijc.30461
98. Marella, N. V., Bhattacharya, S., Mukherjee, L., Xu, J., & Berezney, R. (2009). Cell type specific chromosome territory organization in the interphase nucleus of normal and cancer cells. *Journal of Cellular Physiology*, *221*(1), 130–138. https://doi.org/10.1002/jcp.21836
99. Guo, Y., Xu, Q., Canzio, D., Shou, J., Li, J., Gorkin, D., Jung, I., Wu, H., Zhai, Y., Tang, Y., Lu, Y., Wu, Y., Jia, Z., Li, W., Zhang, M., Ren, B., Krainer, A., Maniatis, T., & Wu, Q. (2015). CRISPR Inversion of CTCF Sites Alters Genome Topology and Enhancer/Promoter Function. *Cell*, *162*(4), 900–910. https://doi.org/10.1016/j.cell.2015.07.038
100. Sanborn, A., Rao, S., Huang, S., Durand, N., Huntley, M., Jewett, A., Bochkov, I., Chinnappan, D., Cutkosky, A., Li, J., Geeting, K., Gnirke, A., Melnikov, A., McKenna, D., Stamenova, E., Lander, E., & Aiden, E. L. (2016). Chromatin Extrusion Explains Key Features of Loop and Domain Formation in Wild-type and Engineered Genomes. *The FASEB Journal*, *30*(S1). https://doi.org/10.1096/fasebj.30.1_supplement.588.1

101. Lettice, L. A. (2003). A long-range Shh enhancer regulates expression in the developing limb and fin and is associated with preaxial polydactyly. *Human Molecular Genetics*, *12*(14), 1725–1735. https://doi.org/10.1093/hmg/ddg180
102. Fukami, M., Tsuchiya, T., Takada, S., Kanbara, A., Asahara, H., Igarashi, A., Kamiyama, Y., Nishimura, G., & Ogata, T. (2012). Complex genomic rearrangement in theSOX95′ region in a patient with Pierre Robin sequence and hypoplastic left scapula. *American Journal of Medical Genetics Part A*, *158A*(7), 1529–1534. https://doi.org/10.1002/ajmg.a.35308
103. Northcott, P. A., Lee, C., Zichner, T., Stütz, A. M., Erkek, S., Kawauchi, D., Shih, D. J. H., Hovestadt, V., Zapatka, M., Sturm, D., Jones, D. T. W., Kool, M., Remke, M., Cavalli, F. M. G., Zuyderduyn, S., Bader, G. D., VandenBerg, S., Esparza, L. A., Ryzhova, M., . . . Pfister, S. M. (2014). Enhancer hijacking activates GFI1 family oncogenes in medulloblastoma. *Nature*, *511*(7510), 428–434. https://doi.org/10.1038/nature13379
104. Taub, R., Kirsch, I., Morton, C., Lenoir, G., Swan, D., Tronick, S., Aaronson, S., & Leder, P. (1982). Translocation of the c-myc gene into the immunoglobulin heavy chain locus in human Burkitt lymphoma and murine plasmacytoma cells. *Proceedings of the National Academy of Sciences*, *79*(24), 7837–7841. https://doi.org/10.1073/pnas.79.24.7837
105. Mitelman, F., Johansson, B., & Mertens, F. (2007). The impact of translocations and gene fusions on cancer causation. Nature Reviews Cancer, 7(4), 233–245. https://doi.org/10.1038/nrc2091
106. Küppers, R. (2005). Mechanisms of B-cell lymphoma pathogenesis. *Nature Reviews Cancer*, *5*(4), 251–262. https://doi.org/10.1038/nrc1589
107. Nussenzweig, A., & Nussenzweig, M. C. (2010). Origin of Chromosomal Translocations in Lymphoid Cancer. *Cell*, *141*(1), 27–38. https://doi.org/10.1016/j.cell.2010.03.016
108. Bouamar, H., Abbas, S., Lin, A. P., Wang, L., Jiang, D., Holder, K. N., Kinney, M. C., Hunicke-Smith, S., & Aguiar, R. C. T. (2013). A capture-sequencing strategy identifies IRF8, EBF1, and APRIL as novel IGH fusion partners in B-cell lymphoma. Blood, 122(5), 726–733. https://doi.org/10.1182/blood-2013-04-495804

109. Pasqualucci, L., Neumeister, P., Goossens, T., Nanjangud, G., Chaganti, R. S. K., Küppers, R., & Dalla-Favera, R. (2001). Hypermutation of multiple proto-oncogenes in B-cell diffuse large-cell lymphomas. *Nature*, *412*(6844), 341–346. https://doi.org/10.1038/35085588
110. Krem, M. M., Press, O. W., Horwitz, M. S., & Tidwell, T. (2015). Mechanisms and clinical applications of chromosomal instability in lymphoid malignancy. *British Journal of Haematology*, *171*(1), 13–28. https://doi.org/10.1111/bjh.13507
111. Knecht, H., Sawan, B., Lichtensztejn, D., Lemieux, B., Wellinger, R. J., & Mai, S. (2008). The 3D nuclear organization of telomeres marks the transition from Hodgkin to Reed–Sternberg cells. *Leukemia*, *23*(3), 565–573. https://doi.org/10.1038/leu.2008.314
112. Guffei, A., Sarkar, R., Klewes, L., Righolt, C., Knecht, H., & Mai, S. (2010). Dynamic chromosomal rearrangements in Hodgkin's lymphoma are due to ongoing three-dimensional nuclear remodeling and breakage-bridge-fusion cycles. *Haematologica*, *95*(12), 2038–2046. https://doi.org/10.3324/haematol.2010.030171
113. Harrison, C. J., Moorman, A. V., Broadfield, Z. J., Cheung, K. L., Harris, R. L., Reza Jalali, G., Robinson, H. M., Barber, K. E., Richards, S. M., Mitchell, C. D., Eden, T. O. B., Hann, I. M., Hill, F. G., Kinsey, S. E., Gibson, B. E., Lilleyman, J., Vora, A., Goldstone, A. H., Franklin, I. M., . . . Martineau, M. (2004). Three distinct subgroups of hypodiploidy in acute lymphoblastic leukaemia. *British Journal of Haematology*, *125*(5), 552–559. https://doi.org/10.1111/j.1365-2141.2004.04948.x
114. Knecht, H., Kongruttanachok, N., Sawan, B., Brossard, J., Prévost, S., Turcotte, E., Lichtensztejn, Z., Lichtensztejn, D., & Mai, S. (2012). Three-dimensional Telomere Signatures of Hodgkin- and Reed-Sternberg Cells at Diagnosis Identify Patients with Poor Response to Conventional Chemotherapy. *Translational Oncology*, *5*(4), 269–277. https://doi.org/10.1593/tlo.12142
115. M'kacher, R., Bennaceur-Griscelli, A., Girinsky, T., Koscielny, S., Delhommeau, F., Dossou, J., Violot, D., Leclercq, E., Courtier, M. H., Béron-Gaillard, N., Assaf, E., Ribrag, V., Bourhis, J., Feneux, D., Bernheim, A., Parmentier, C., & Carde, P. (2007). Telomere Shortening and Associated Chromosomal Instability in Peripheral Blood Lymphocytes of Patients With Hodgkin's Lymphoma Prior to Any Treatment Are

Predictive of Second Cancers. *International Journal of Radiation Oncology*Biology*Physics*, *68*(2), 465–471. https://doi.org/10.1016/j.ijrobp.2007.01.050

116. Lobetti-Bodoni, C., Bernocco, E., Genuardi, E., Boccadoro, M., & Ladetto, M. (2010). Telomeres and telomerase in normal and malignant B-cells. *Hematological Oncology*, *28*(4), 157–167. https://doi.org/10.1002/hon.937

117. Dubik, N., & Mai, S. (2020). Lamin A/C: Function in Normal and Tumor Cells. *Cancers*, *12*(12), 3688. https://doi.org/10.3390/cancers12123688

118. Guilly, M. N., Kolb, J. P., Gosti, F., Godeau, F., & Courvalin, J. C. (1990). Lamins A and C are not expressed at early stages of human lymphocyte differentiation. *Experimental Cell Research*, *189*(1), 145–147. https://doi.org/10.1016/0014-4827(90)90267-e

119. Prokocimer, M., Margalit, A., & Gruenbaum, Y. (2006). The nuclear lamina and its proposed roles in tumorigenesis: Projection on the hematologic malignancies and future targeted therapy. *Journal of Structural Biology*, *155*(2), 351–360. https://doi.org/10.1016/j.jsb.2006.02.016

120. González-Granado, J. M., Silvestre-Roig, C., Rocha-Perugini, V., Trigueros-Motos, L., Cibrián, D., Morlino, G., Blanco-Berrocal, M., Osorio, F. G., Freije, J. M. P., López-Otín, C., Sánchez-Madrid, F., & Andrés, V. (2014). Nuclear Envelope Lamin-A Couples Actin Dynamics with Immunological Synapse Architecture and T Cell Activation. *Science Signaling*, *7*(322). https://doi.org/10.1126/scisignal.2004872

121. Contu, F., Rangel-Pozzo, A., Trokajlo, P., Wark, L., Klewes, L., Johnson, N., Petrogiannis-Haliotis, T., Gartner, J., Garini, Y., Vanni, R., Knecht, H., & Mai, S. (2018). Distinct 3D Structural Patterns of Lamin A/C Expression in Hodgkin and Reed-Sternberg Cells. *Cancers*, *10*(9), 286. https://doi.org/10.3390/cancers10090286

122. Agrelo, R., Setien, F., Espada, J., Artiga, M. J., Rodriguez, M., Pérez-Rosado, A., Sanchez-Aguilera, A., Fraga, M. F., Piris, M. A., & Esteller, M. (2005). Inactivation of theLamin A/CGene by CpG Island Promoter Hypermethylation in Hematologic Malignancies, and Its Association With Poor Survival in Nodal Diffuse Large B-Cell Lymphoma. *Journal of Clinical Oncology*, *23*(17), 3940–3947. https://doi.org/10.1200/jco.2005.11.650

123. Foster, C. R., Robson, J. L., Simon, W. J., Twigg, J., Cruikshank, D., Wilson, R. G., & Hutchison, C. J. (2011). The role of Lamin A in cytoskeleton organization in colorectal cancer cells. *Nucleus*, *2*(5), 434–443. https://doi.org/10.4161/nucl.2.5.17775
124. Moss, S. F., Krivosheyev, V., de Souza, A., Chin, K., Gaetz, H. P., Chaudhary, N., Worman, H. J., & Holt, P. R. (1999). Decreased and aberrant nuclear lamin expression in gastrointestinal tract neoplasms. *Gut*, *45*(5), 723–729. https://doi.org/10.1136/gut.45.5.723
125. Dasari, S., & Bernard Tchounwou, P. (2014). Cisplatin in cancer therapy: Molecular mechanisms of action. *European Journal of Pharmacology*, *740*, 364–378. https://doi.org/10.1016/j.ejphar.2014.07.025
126. Wordeman, L., & Vicente, J. J. (2021). Microtubule Targeting Agents in Disease: Classic Drugs, Novel Roles. *Cancers*, *13*(22), 5650. https://doi.org/10.3390/cancers13225650
127. Dziadkowiec, K. N., Gąsiorowska, E., Nowak-Markwitz, E., & Jankowska, A. (2016). PARP inhibitors: review of mechanisms of action and BRCA1/2 mutation targeting. *Menopausal Review*, *4*, 215–219. https://doi.org/10.5114/pm.2016.65667
128. El-Daly, H., Kull, M., Zimmermann, S., Pantic, M., Waller, C. F., & Martens, U. M. (2005). Selective cytotoxicity and telomere damage in leukemia cells using the telomerase inhibitor BIBR1532. *Blood*, *105*(4), 1742–1749. https://doi.org/10.1182/blood-2003-12-4322
129. Damm, K. (2001). A highly selective telomerase inhibitor limiting human cancer cell proliferation. *The EMBO Journal*, *20*(24), 6958–6968. https://doi.org/10.1093/emboj/20.24.6958
130. Willemze, R. (2005). WHO-EORTC classification for cutaneous lymphomas. *Blood*, *105*(10), 3768–3785. https://doi.org/10.1182/blood-2004-09-3502
131. Bekkenk, M. W., Geelen, F. A. M. J., Vader, P. C. V. V., Heule, F., Geerts, M. L., van Vloten, W. A., Meijer, C. J. L. M., & Willemze, R. (2000). Primary and secondary cutaneous CD30+lymphoproliferative disorders: a report from the Dutch Cutaneous Lymphoma Group on the long-term follow-up data of 219 patients and guidelines for diagnosis and treatment. *Blood*, *95*(12), 3653–3661. https://doi.org/10.1182/blood.v95.12.3653

132. Böni, R., Xin, H., Kamarashev, J., Utzinger, E., Dummer, R., Kempf, W., Burg, G., & Kutzner, H. (2000). Allelic Deletion at 9p21–22 in Primary Cutaneous CD30+ Large Cell Lymphoma. *Journal of Investigative Dermatology*, *115*(6), 1104–1107. https://doi.org/10.1038/jid.2000.4
133. Mao, X., Orchard, G., Lillington, D. M., Russell-Jones, R., Young, B. D., & Whittaker, S. (2003). Genetic alterations in primary cutaneous CD30+ anaplastic large cell lymphoma. *Genes, Chromosomes and Cancer*, *37*(2), 176–185. https://doi.org/10.1002/gcc.10184
134. van Kester, M. S., Tensen, C. P., Vermeer, M. H., Dijkman, R., Mulder, A. A., Szuhai, K., Willemze, R., & van Doorn, R. (2010). Cutaneous Anaplastic Large Cell Lymphoma and Peripheral T-Cell Lymphoma NOS Show Distinct Chromosomal Alterations and Differential Expression of Chemokine Receptors and Apoptosis Regulators. *Journal of Investigative Dermatology*, *130*(2), 563–575. https://doi.org/10.1038/jid.2009.270
135. Chevret, E., Andrique, L., Prochazkova-Carlotti, M., Ferrer, J., Cappellen, D., Laharanne, E., Idrissi, Y., Boettiger, A., Sahraoui, W., Ruiz, F., Pham-Ledard, A., Vergier, B., Belloc, F., Dubus, P., Beylot-Barry, M., & Merlio, J. P. (2014). Telomerase functions beyond telomere maintenance in primary cutaneous T-cell lymphoma. *Blood*, *123*(12), 1850–1859. https://doi.org/10.1182/blood-2013-05-500686
136. Bienz, M. N., Petrogiannis-Haliotis, T., Pehr, K., Benlimame, N., Mai, S., & Knecht, H. (2021). Three-Dimensional Telomeric Fingerprint of Mycosis Fungoides and/or Sézary Syndrome: A Pilot Study. Journal of Investigative Dermatology, 141(6), 1598–1601.e4. https://doi.org/10.1016/j.jid.2020.09.032
137. Davis, T. H., Morton, C. C., Miller-Cassman, R., Balk, S. P., & Kadin, M. E. (1992). Hodgkin's Disease, Lymphomatoid Papulosis, and Cutaneous T-Cell Lymphoma Derived from a Common T-Cell Clone. *New England Journal of Medicine*, *326*(17), 1115–1122. https://doi.org/10.1056/nejm199204233261704
138. Ehrentraut, S., Nagel, S., Scherr, M., Schneider, B., Quentmeier, H., Geffers, R., Prochorec-Sobieszek, M., Ketterling, R. P., Knudson, R. A., Feldman, A. L., Kadin, M., Drexler, H. G., & MacLeod, R. A. (2012). T(8;9)(p22;p24)/PCM1-JAK2 Activates

SOCS2 and SOCS3 Via STAT5. *Blood*, *120*(21), 1567. https://doi.org/10.1182/blood.v120.21.1567.1567

139. Ehrentraut, S., Schneider, B., Nagel, S., Pommerenke, C., Quentmeier, H., Geffers, R., Feist, M., Kaufmann, M., Meyer, C., Kadin, M. E., Drexler, H. G., & MacLeod, R. A. F. (2016). Th17 cytokine differentiation and loss of plasticity after SOCS1 inactivation in a cutaneous T-cell lymphoma. *Oncotarget*, *7*(23), 34201–34216. https://doi.org/10.18632/oncotarget.9077

140. Wood, A. M., Danielsen, J. M. R., Lucas, C. A., Rice, E. L., Scalzo, D., Shimi, T., Goldman, R. D., Smith, E. D., le Beau, M. M., & Kosak, S. T. (2014). TRF2 and lamin A/C interact to facilitate the functional organization of chromosome ends. Nature Communications, 5(1). https://doi.org/10.1038/ncomms6467

141. Levi, E., Wang, Z., Petrogiannis-Haliotis, T., Pfeifer, W. M., Kempf, W., Drews, R., & Kadin, M. E. (2000). Distinct Effects of CD30 and Fas Signaling in Cutaneous Anaplastic Lymphomas: A Possible Mechanism for Disease Progression. *Journal of Investigative Dermatology*, *115*(6), 1034–1040. https://doi.org/10.1046/j.1523-1747.2000.00175.x

142. Knaus, P. I., Lindemann, D., DeCoteau, J. F., Perlman, R., Yankelev, H., Hille, M., Kadin, M. E., & Lodish, H. F. (1996). A dominant inhibitory mutant of the type II transforming growth factor beta receptor in the malignant progression of a cutaneous T-cell lymphoma. *Molecular and Cellular Biology*, *16*(7), 3480–3489. https://doi.org/10.1128/mcb.16.7.3480

143. Volkenandt, M., Bertino, J. R., Shenoy, B., Koch, O. M., & Kadin, M. E. (1993). Molecular evidence for a clonal relationship between lymphomatoid papulosis and Ki-1 positive large cell anaplastic lymphoma. Journal of Dermatological Science, 6(2), 121–126. https://doi.org/10.1016/0923-1811(93)90001-6

144. Csikesz, C. R., Knudson, R. A., Greipp, P. T., Feldman, A. L., & Kadin, M. (2013). Primary Cutaneous CD30-Positive T-Cell Lymphoproliferative Disorders with Biallelic Rearrangements of DUSP22. Journal of Investigative Dermatology, 133(6), 1680–1682. https://doi.org/10.1038/jid.2013.22

145. Knecht, H., and Mai, S. (2017). The Use of 3D Telomere FISH for the Characterization of the Nuclear Architecture in EBV-Positive Hodgkin's Lymphoma. Methods Mol. Biol. Clifton NJ 1532, 93–104
146. Schaefer, L. H., Schuster, D., & Herz, H. (2001). Generalized approach for accelerated maximum likelihood-based image restoration applied to three-dimensional fluorescence microscopy. Journal of Microscopy, 204(2), 99–107. https://doi.org/10.1046/j.1365-2818.2001.00949.x
147. R Core Team (2021). R: A language and environment for statistical computing. R Foundation for Statistical Computing, Vienna, Austria. URL https://www.R-project.org/
148. RStudio Team. (2021). RStudio: Integrated Development Environment for R. Boston, MA. Retrieved from http://www.rstudio.com/
149. de Vos, W. H., Hoebe, R. A., Joss, G. H., Haffmans, W., Baatout, S., van Oostveldt, P., & Manders, E. M. M. (2009). Controlled light exposure microscopy reveals dynamic telomere microterritories throughout the cell cycle. Cytometry Part A, 75A(5), 428–439. https://doi.org/10.1002/cyto.a.20699
150. Mathur, S., Glogowska, A., McAvoy, E., Righolt, C., Rutherford, J., Willing, C., Banik, U., Ruthirakuhan, M., Mai, S., & Garcia, A. (2014). Three-Dimensional Quantitative Imaging of Telomeres in Buccal Cells Identifies Mild, Moderate, and Severe Alzheimer's Disease Patients. Journal of Alzheimer's Disease, 39(1), 35–48. https://doi.org/10.3233/jad-130866
151. Knecht, H., Righolt, C., & Mai, S. (2013). Genomic Instability: The Driving Force behind Refractory/Relapsing Hodgkin's Lymphoma. Cancers, 5(4), 714–725. https://doi.org/10.3390/cancers5020714
152. Gadji, M., Adebayo Awe, J., Rodrigues, P., Kumar, R., Houston, D. S., Klewes, L., Dièye, T. N., Rego, E. M., Passetto, R. F., de Oliveira, F. M., & Mai, S. (2012). Profiling Three-Dimensional Nuclear Telomeric Architecture of Myelodysplastic Syndromes and Acute Myeloid Leukemia Defines Patient Subgroups. Clinical Cancer Research, 18(12), 3293–3304. https://doi.org/10.1158/1078-0432.ccr-12-0087
153. Adebayo Awe, J., Xu, M. C., Wechsler, J., Benali-Furet, N., Cayre, Y. E., Saranchuk, J., Drachenberg, D., & Mai, S. (2013). Three-Dimensional Telomeric Analysis of Isolated

Circulating Tumor Cells (CTCs) Defines CTC Subpopulations. Translational Oncology, 6(1), 51-IN4. https://doi.org/10.1593/tlo.12361

154. Raz, V., Vermolen, B. J., Garini, Y., Onderwater, J. J. M., Mommaas-Kienhuis, M. A., Koster, A. J., Young, I. T., Tanke, H., & Dirks, R. W. (2008). The nuclear lamina promotes telomere aggregation and centromere peripheral localization during senescence of human mesenchymal stem cells. Journal of Cell Science, 121(24), 4018–4028. https://doi.org/10.1242/jcs.034876

155. Mounkes, L. C., & Stewart, C. L. (2004). Aging and nuclear organization: lamins and progeria. Current Opinion in Cell Biology, 16(3), 322–327. https://doi.org/10.1016/j.ceb.2004.03.009

156. Mai, S., & Garini, Y. (2006). The significance of telomeric aggregates in the interphase nuclei of tumor cells. Journal of Cellular Biochemistry, 97(5), 904–915. https://doi.org/10.1002/jcb.20760

157. Rengstl, B., Newrzela, S., Heinrich, T., Weiser, C., Thalheimer, F. B., Schmid, F., Warner, K., Hartmann, S., Schroeder, T., Küppers, R., Rieger, M. A., & Hansmann, M. L. (2013). Incomplete cytokinesis and re-fusion of small mononucleated Hodgkin cells lead to giant multinucleated Reed–Sternberg cells. Proceedings of the National Academy of Sciences, 110(51), 20729–20734. https://doi.org/10.1073/pnas.1312509110

158. Huang, S., Risques, R. A., Martin, G. M., Rabinovitch, P. S., & Oshima, J. (2008). Accelerated telomere shortening and replicative senescence in human fibroblasts overexpressing mutant and wild-type lamin A. Experimental Cell Research, 314(1), 82–91. https://doi.org/10.1016/j.yexcr.2007.08.004

159. Gonzalez-Suarez, I., Redwood, A. B., Perkins, S. M., Vermolen, B., Lichtensztejin, D., Grotsky, D. A., Morgado-Palacin, L., Gapud, E. J., Sleckman, B. P., Sullivan, T., Sage, J., Stewart, C. L., Mai, S., & Gonzalo, S. (2009). Novel roles for A-type lamins in telomere biology and the DNA damage response pathway. The EMBO Journal, 28(16), 2414–2427. https://doi.org/10.1038/emboj.2009.196

160. Zeng, Y., & Feldman, A. L. (2015). Genetics of anaplastic large cell lymphoma. Leukemia & Lymphoma, 57(1), 21–27. https://doi.org/10.3109/10428194.2015.1064530

161. Domcke, S., Sinha, R., Levine, D. A., Sander, C., & Schultz, N. (2013). Evaluating cell lines as tumour models by comparison of genomic profiles. *Nature Communications*, *4*(1). https://doi.org/10.1038/ncomms3126
162. Chen, B., Sirota, M., Fan-Minogue, H., Hadley, D., & Butte, A. J. (2015). Relating hepatocellular carcinoma tumor samples and cell lines using gene expression data in translational research. *BMC Medical Genomics*, *8*(S2). https://doi.org/10.1186/1755-8794-8-s2-s5